ARTICLES
https://doi.org/10.1038/s41593-019-0380-9

nature neuroscience

Corrected: Publisher Correction

Neuronal deletion of *Gtf2i*, associated with Williams syndrome, causes behavioral and myelin alterations rescuable by a remyelinating drug

Boaz Barak[1,2,3*], Zicong Zhang[4], Yuanyuan Liu[4], Ariel Nir[3], Sari S. Trangle[2], Michaela Ennis[1], Kirsten M. Levandowski[5], Dongqing Wang[1], Kathleen Quast[1], Gabriella L. Boulting[6], Yi Li[4], Dashzeveg Bayarsaihan[7], Zhigang He[4*] and Guoping Feng[1,5*]

Williams syndrome (WS), caused by a heterozygous microdeletion on chromosome 7q11.23, is a neurodevelopmental disorder characterized by hypersociability and neurocognitive abnormalities. Of the deleted genes, general transcription factor IIi (*Gtf2i*) has been linked to hypersociability in WS, although the underlying mechanisms are poorly understood. We show that selective deletion of *Gtf2i* in the excitatory neurons of the forebrain caused neuroanatomical defects, fine motor deficits, increased sociability and anxiety. Unexpectedly, 70% of the genes with significantly decreased messenger RNA levels in the mutant mouse cortex are involved in myelination, and mutant mice had reduced mature oligodendrocyte cell numbers, reduced myelin thickness and impaired axonal conductivity. Restoring myelination properties with clemastine or increasing axonal conductivity rescued the behavioral deficits. The frontal cortex from patients with WS similarly showed reduced myelin thickness, mature oligodendrocyte cell numbers and mRNA levels of myelination-related genes. Our study provides molecular and cellular evidence for myelination deficits in WS linked to neuronal deletion of *Gtf2i*.

Williams syndrome (WS) is a multisystemic neurodevelopmental disorder characterized by hypersociability with unique cognitive and personality profiles[1,2]. These include intellectual disability, distinct overfriendliness, increased empathy and elevated anxiety derived from fear and specific phobias[2]. WS is caused by haploinsufficiency of about 26 genes from the WS chromosome region (WSCR) at chromosome 7q11.23. While approximately 95% of patients with WS have a hemizygous deletion of the entire WSCR, the other approximately 5% of patients have atypical microdeletions that may only affect a few genes of the WSCR[3–6] and thus are helpful in defining genetic links to certain symptoms. In particular, atypical microdeletions that overlap with *GTF2I* and GTF2I repeat domain containing 1 (*GTF2IRD1*), which are members of the general transcription factor 2I gene family, affect the cognitive phenotype in patients with WS[3,4,6]. Rare cases of individuals with microdeletions that affect either gene, but not both, strongly indicated that *GTF2IRD1* disruption is associated with WS craniofacial dysmorphism and cognitive deficits, whereas *GTF2I* deletion may contribute to WS social behaviors and mental impairment[4,5].

GTF2I encodes the general transcription factor II-I (TFII-I) protein, a highly conserved and ubiquitously expressed multifunctional transcription factor that regulates gene expression through interactions with tissue-specific transcription factors and complexes related to chromatin remodeling[7]. Previous work on mouse models for WS[8] studied the role of *Gtf2i* deletion by using either heterozygous mice with the majority of the WSCR[9] deleted, partial WSCR deletions[10] or single-gene deletion models[11–13]. These studies showed correlations between *Gtf2i* haploinsufficiency and certain WS-relevant behavioral phenotypes, including hypersociability and social dishabituation. Homozygous *Gtf2i* knockout mice are embryonically lethal, mainly due to failed neural tube closure[12–14]. Thus, the neuronal function of the *Gtf2i* gene and its role in the molecular and cellular mechanisms underlying WS behavioral and neurodevelopmental phenotypes remain completely unknown. In this study, we selectively deleted *Gtf2i* in the excitatory neurons of the forebrain and characterized molecular, cellular and behavioral changes in the brain. We found that forebrain excitatory neuron-specific *Gtf2i* knockout mice show WS-relevant abnormalities, including neuroanatomical defects, fine motor deficits, increased sociability and anxiety. Surprisingly, RNA sequencing (RNA-Seq) analysis revealed that 70% of the genes with significantly decreased mRNA level were involved in myelination. Furthermore, we found reduced numbers of mature oligodendrocytes, reduced myelin thickness and impaired axonal conductivity. We further showed that normalization of impaired myelination properties or axonal conductivity rescues behavioral deficits. Importantly, similar myelination defects were also found in the postmortem human frontal cortex of patients with WS. Together, these data implicate myelination, linked to neuronal loss of *Gtf2i*, as an important pathophysiology in WS and point to new paths for exploring potential therapeutic targets.

Results

***Gtf2i* deletion in the excitatory neurons of the forebrain causes neuroanatomical and behavioral alterations.** To dissect the function of *Gtf2i* in neurons, we crossed *Gtf2i loxP* mice[15] with NEX-Cre mice[16], a Cre line that expresses Cre recombinase selectively in the

[1]McGovern Institute for Brain Research and Department of Brain & Cognitive Sciences, MIT, Cambridge, MA, USA. [2]The School of Psychological Sciences, Faculty of Social Sciences, Tel Aviv University, Tel Aviv, Israel. [3]The Sagol School of Neuroscience, Tel Aviv University, Tel Aviv, Israel. [4]F.M. Kirby Neurobiology Center, Boston Children's Hospital and Department of Neurology, Harvard Medical School, Boston, MA, USA. [5]Stanley Center for Psychiatric Research, Broad Institute of MIT and Harvard, Cambridge, MA, USA. [6]Department of Neurobiology, Harvard Medical School, Boston, MA, USA. [7]Department of Reconstructive Sciences, University of Connecticut, Farmington, CT, USA. *e-mail: boazba@tauex.tau.ac.il; zhigang.he@childrens.harvard.edu; fengg@mit.edu

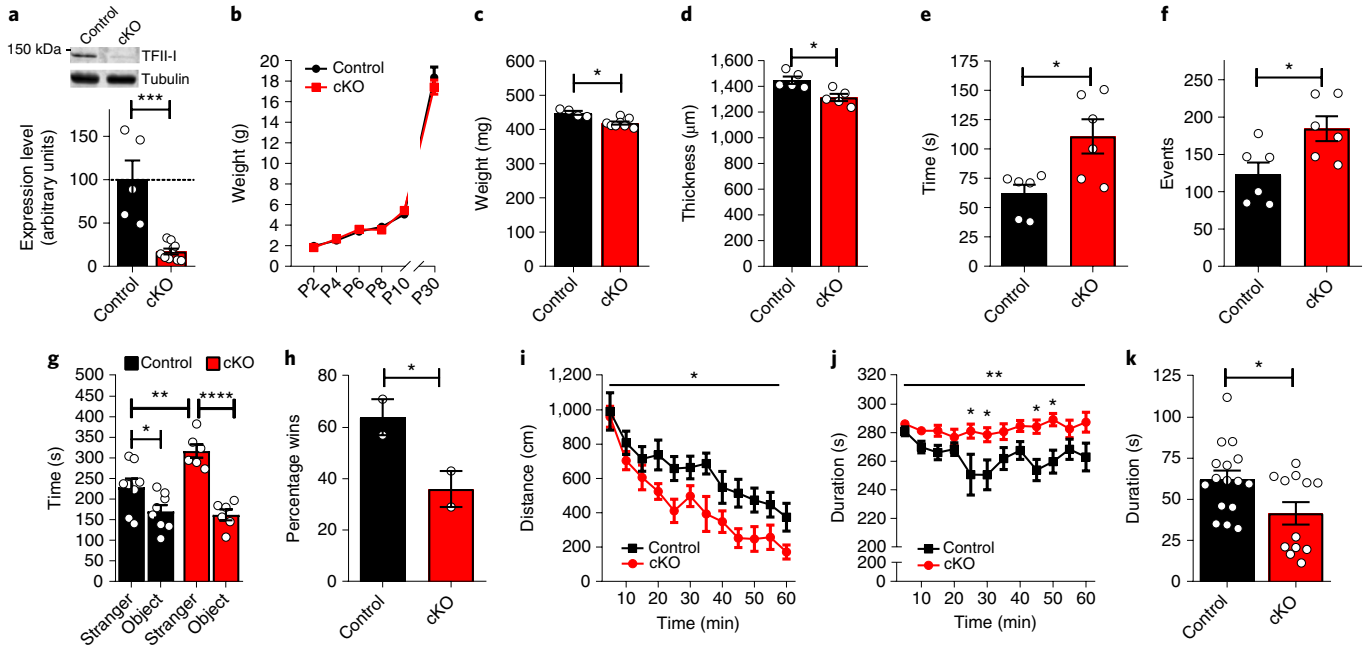

Fig. 1 | Neuroanatomical and behavioral deficits in *Gtf2i* cKO mice. a, Significantly reduced expression of TFII-I in whole cortex of 1-month-old cKO mice compared to controls, as measured by western blot. The image has been cropped from a full western blot ($P=0.001$). **b**, cKO mice have similar body weight compared to controls. **c**,**d**, One-month-old cKO mice have significantly reduced brain weight ($P=0.0162$) (**c**) and cortical thickness ($P=0.0159$) (**d**) compared to controls. **e**,**f**, Increased levels of social behavior in cKO mice compared to controls as demonstrated by significantly longer duration ($P=0.03$) (**e**, dyadic interaction time) and higher frequency of close social interaction events ($P=0.0476$) (**f**, dyadic social events) during the dyadic social interaction test. **g**, In the three-chambered social interaction test, when looking at social preference duration, cKO mice showed significantly higher social preference compared to controls, interacting significantly longer with a stranger mouse compared to controls (*$P=0.04$, **$P=0.0086$, ****$P<0.0001$). **h**, Decreased levels of social dominance in cKO mice, demonstrated by a significantly lower percentage of wins in the tube test compared to controls ($P=0.0392$). **i**–**k**, cKO mice showed significantly increased levels of anxiety-like behaviors compared to controls as demonstrated by significantly shorter total exploration distance in the open field exploration test ($P=0.0108$) (**i**), significantly longer duration in the margins of the open arena ($P=0.0024$) (**j**) and significantly less time in the open arms of an elevated zero maze ($P=0.043$) (**k**) compared to controls. *$P<0.05$, **$P<0.01$, ***$P<0.005$, ****$P<0.0001$, two-tailed *t*-test (**a**,**c**–**h**,**k**), two-way repeated-measures ANOVA with Bonferroni post hoc test (**b**,**i**,**j**). Data are shown as mean ± s.e.m. **a**–**d**, $n=8$ control, $n=10$ cKO. **e**–**g**, $n=8$ control pairs, $n=8$ cKO pairs. **h**–**k**, $n=10$ control, $n=10$ cKO. See Supplementary Fig. 2A for gel source data.

excitatory neurons of the forebrain (Supplementary Fig.1) starting around embryonic day (E) 11.5 (ref. [16]). The resulting mice, referred herein as cKO (*Gtf2i*$^{f/f}$:NEX-Cre$^{+/-}$), had homozygous deletion of *Gtf2i* selectively in the excitatory neurons of the forebrain (Fig. 1a and Supplementary Figs. 2 and 3).

Patients with WS show altered brain volume and cortical anatomical properties[17–19]. Therefore, we examined whether deletion of *Gtf2i* from the excitatory neurons in the forebrain is sufficient to cause neuroanatomical abnormalities. While cKOs showed normal body weight compared to control (*Gtf2i*$^{f/f}$:NEX-Cre$^{-/-}$) littermates (Fig. 1b), 1-month-old cKO mice showed significantly reduced brain weight (Fig. 1c) and cortical thickness compared to controls (Fig. 1d and Supplementary Fig. 4A,B).

Behaviorally, cKO mice demonstrated significantly higher levels of social behavior as assessed in three different social behavior-related tests. Specifically, compared to controls, 23-day-old cKO mice showed significantly longer duration (Fig. 1e and Supplementary Fig. 5A) and significantly higher frequency (Fig. 1f and Supplementary Fig. 5B) in close interaction in the dyadic social interaction test. In the social preference test, 1-month-old cKO mice showed significantly higher preference to interact with a stranger mouse than with an object compared to controls (Fig. 1g). cKO mice also exhibited significantly decreased social dominance, as demonstrated by a significantly lower win percentage than controls during matches with a stranger mouse in the tube test (Fig. 1h). Because heightened non-social anxiety is a prominent feature of WS[1], we tested mice for anxiety-like behaviors in an open field exploration test (Fig. 1i,j and Supplementary Fig. 6A–C) and elevated zero maze test (Fig. 1k). We found significantly higher levels of non-social anxiety-like behaviors in cKO mice compared to controls. No other significant behavioral differences were found in cKO mice compared to controls (Supplementary Fig.7). These data suggest that *Gtf2i* deletion in the excitatory neurons of the forebrain is sufficient to induce hypersociability and increased levels of non-social anxiety, resembling some core phenotypes found in patients with WS.

***Gtf2i* neuronal deletion affects myelination-related transcriptomic and cellular properties.** To discover the altered molecular processes that may underlie the behavioral and anatomical abnormalities in cKO mice, we performed RNA-Seq on the whole cortex of cKO mice and their controls. To characterize the transcriptional abnormalities in a developmental manner, we used 1-day-old (Supplementary Fig. 8 and Supplementary Table 1) and 1-month-old mice (Fig. 2a–c, Supplementary Fig. 9 and Supplementary Table 1). Surprisingly, although *Gtf2i* was selectively deleted in excitatory neurons, 70% of the genes with a significantly lower mRNA level in the cortex of 1-month-old cKO mice were involved in myelin development and function (Fig. 2a–c and Supplementary Table 1)[20]. These genes encode proteins involved in the development, differentiation and function of oligodendrocytes[21–23], and play key roles in the formation, maintenance and functionality of myelin

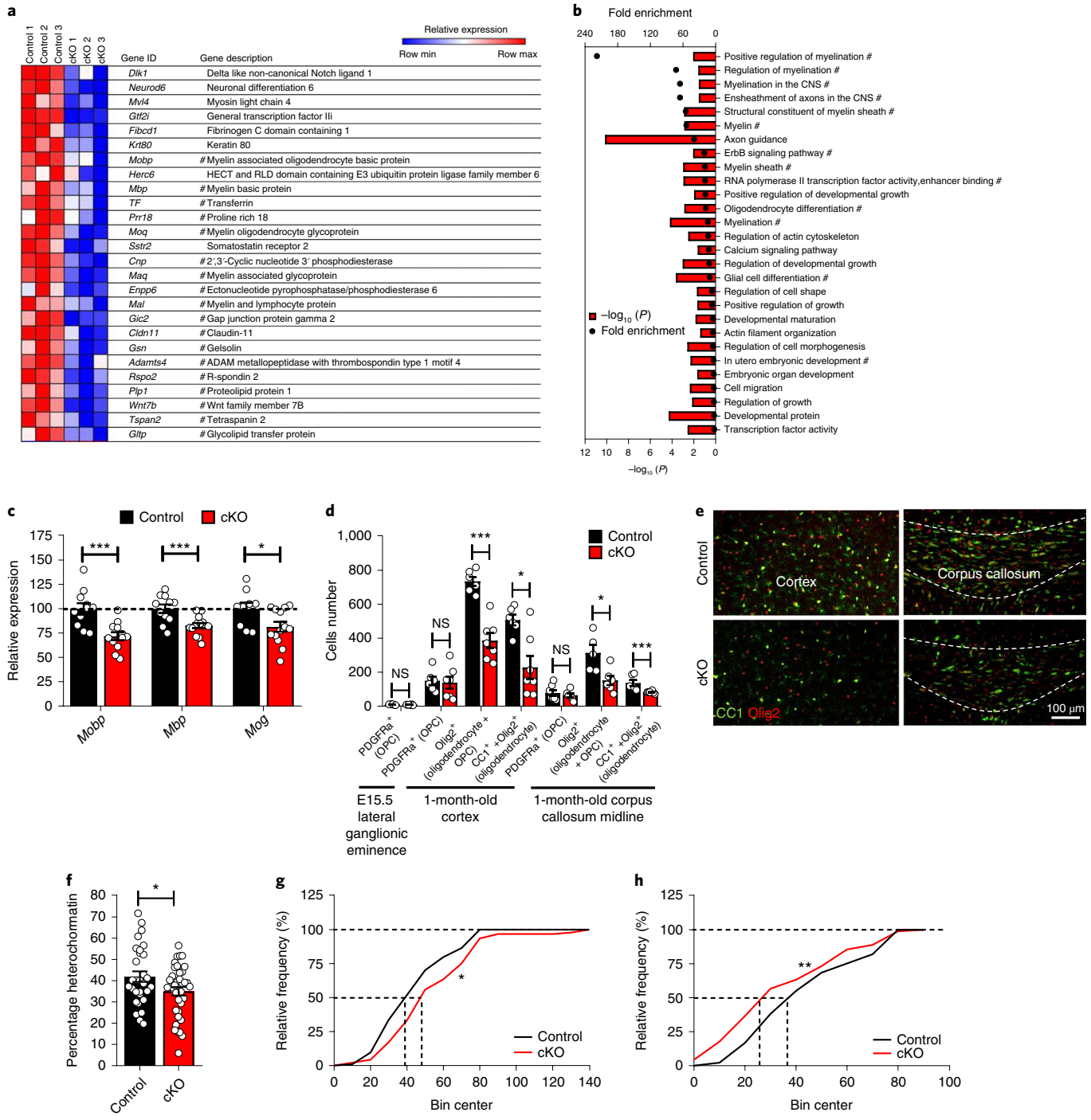

Fig. 2 | Myelination-related transcriptomic and cellular alterations in *Gtf2i* cKO mice. a, Gene expression heatmap table including all the genes with significantly decreased mRNA level in the cortex of 1-month-old cKO mice compared to controls. Myelination-related genes are labeled with a hash symbol. **b**, Significantly downregulated cellular pathways in the cortex of 1-month-old cKO mice compared to controls. Myelination-related pathways are labeled with a hash symbol (#). **c**, Reduced mRNA level of myelin-related genes in the cortex of cKO mice is validated by qPCR (myelin associated oligodendrocyte basic protein (*Mobp*), ***$P=0.0006$; myelin basic protein (*Mbp*), ***$P=0.0015$; myelin oligodendrocyte glycoprotein (*Mog*), *$P=0.031$). **d**, No significant difference in the number of OPCs in E15.5 cKO embryos compared to controls was noted. In the cortex and midline of the corpus callosum of 1-month-old cKO mice, the number of oligodendrocytes was significantly reduced, while the number of OPCs was not altered (cortex, *$P=0.022$, ***$P=0.0012$; corpus callosum, *$P=0.0173$, ***$P=0.0022$). **e**, Representative images of immunofluorescence labeling demonstrating reduced number of oligodendrocytes in the cortex and midline of the corpus callosum of 1-month-old cKO mice compared to controls. This experiment was repeated independently in six pairs of mice with similar results. **f**, Significantly reduced oligodendrocyte nuclear heterochromatin percentage in the midline of the corpus callosum of 1-month-old cKO mice compared to controls ($P=0.0342$). **g**, Histone H3ac intensity in oligodendrocytes in the cortex of cKO mice is significantly higher compared to controls ($P=0.0352$). **h**, Histone H3K9me3 intensity in oligodendrocytes in cKO mice cortex is significantly lower compared to controls ($P=0.0061$). *$P<0.05$, **$P<0.01$, ***$P<0.005$. Fisher's exact test (**b**), two-tailed *t*-test (**c**,**d**,**f**) and two-sided Kolmogorov–Smirnov test (**g**,**h**). Data are shown as the mean ± s.e.m. **a**,**b**, $n=3$ controls, $n=3$ cKO mice. **c**, $n=11$ controls, $n=11$ cKO mice. **d**, $n=7$ controls, $n=7$ cKO mice, for both E15.5 and 1-month-old mice. **f**, $n=30$ nuclei from control mice, $n=37$ nuclei from cKO mice. **g**, $n=90$ nuclei from control mice, $n=90$ nuclei from cKO mice. **h**, $n=104$ nuclei from control mice, $n=93$ nuclei from cKO mice.

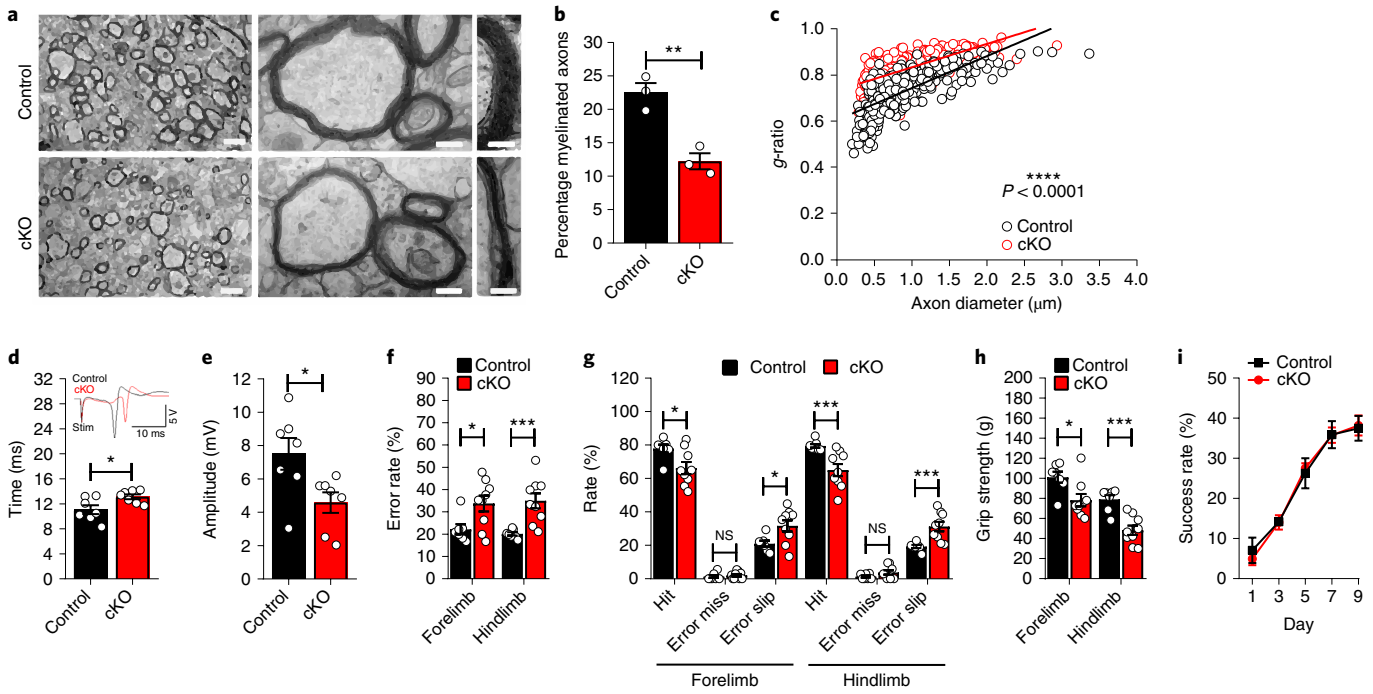

Fig. 3 | *Gtf2i* cKO mice show impaired myelin ultrastructure, neuronal conductivity and motor skills. a, Representative images of myelin ultrastructural abnormalities in the midline of the corpus callosum of cKO mice compared to controls. This experiment was repeated independently in three pairs of mice with similar results. Scale bars: left = 1,500 nm; middle = 300 nm; right = 100 nm. **b**, Significantly lower percentage of myelinated axons in the midline of the corpus callosum of cKO mice compared to controls ($P = 0.0064$). **c**, Significantly reduced myelin thickness in the midline of the corpus callosum of cKO mice, as measured by an increased *g*-ratio in cKO mice compared to controls. **d**,**e**, Neuronal conductivity deficits in the corpus callosum of cKO mice, demonstrated by significantly longer response latency (**d**, insets are representative traces of evoked field potentials, ($P = 0.0238$)) and lower peak amplitude of evoked field potentials (**e**) in cKO mice compared to controls ($P = 0.0247$). **f**,**g**, Fine motor deficits in cKO mice (**f**) compared to controls ($^*P = 0.042$, $^{***}P = 0.0007$) (**g**) demonstrated by a significantly higher error rate from cKO mice for both forelimb and hindlimb in the horizontal irregular ladder walking test (forelimb, hit $^*P = 0.0311$, error slip $^*P = 0.042$; hindlimb, hit $^{***}P = 0.0021$, error slip $^{***}P = 0.0007$). **h**, Reduced paw grip strength of both forelimb and hindlimb in cKO mice compared to controls ($^*P = 0.0214$, $^{***}P = 0.0021$). **i**, No significant difference between cKO mice and controls in the single-pellet food retrieval task during the learning phase ($P = 0.97$). **b**–**h**, $^*P < 0.05$, $^{**}P < 0.01$, $^{***}P < 0.005$, $^{****}P < 0.0001$. Two-tailed *t*-test (**b**–**h**), two-way repeated measures ANOVA with Bonferroni post hoc test (**i**). Data are shown as mean ± s.e.m. **b**, $n = 3$ controls, $n = 3$ cKO mice. **c**, $n = 365$ axons from 3 control mice, $n = 405$ axons from 3 cKO mice. **d**,**e**, $n = 7$ controls, $n = 7$ cKO mice. **f**–**h**, $n = 7$ controls, $n = 9$ cKO mice. **i**, $n = 4$ controls, $n = 9$ cKO mice.

sheaths[24]. Computationally, in mice these genes were found to be significantly enriched in myelinating oligodendrocytes, but not in oligodendrocyte precursor cells (OPCs) (Supplementary Fig. 10, upper row), indicating a potential non-cell autonomous effect of neuronal *Gtf2i* deletion on oligodendrocytes.

To examine how lower mRNA level of these genes might be reflected in the development of oligodendrocyte-related cell populations, we quantified the number of OPCs and oligodendrocytes in cKO mice. Of special note, it was previously shown that Cre recombinase is not active in oligodendrocytes in NEX-Cre mice[16]; we confirmed this finding using a Cre reporter line (Supplementary Fig. 11). We further confirmed that TFII-I expression was normal in the oligodendrocytes of cKO mice (Supplementary Figs. 12,13). In E15.5 cKO embryos, no significant difference was found in OPC number in the lateral ganglionic eminence compared to controls (Fig. 2d). Similarly, no significant difference was found in OPC number in the cortex and midline of the corpus callosum between 1-month-old cKO mice and their controls (Fig. 2d). However, the number of oligodendrocytes in the cortex and midline of the corpus callosum of 1-month-old cKO mice was significantly reduced compared to that of controls (Fig. 2d,e).

To test whether the reduced number of oligodendrocytes was a result of lack of oligodendrocyte maturation, we analyzed nuclear chromatin condensation[25]. Oligodendrocytes in the midline of the corpus callosum of 1-month-old cKO mice had a significantly lower proportion of nuclear heterochromatin (Fig. 2f and Supplementary Fig.14). There were also significantly higher levels of histone acetylation (Fig. 2g and Supplementary Fig.15) and significantly lower levels of repressive histone methylation marks (Fig. 2h and Supplementary Fig.15) in the cortex of cKO mice compared to controls, all of which are known to be essential for oligodendrocyte differentiation and chromatin compaction[25–27].

***Gtf2i* neuronal deletion impairs myelin ultrastructure, neuronal conductivity and motor skills.** We next investigated whether these molecular and cellular deficits affect myelin structure and function. Analysis of myelin ultrastructure (Fig. 3a) revealed a significantly lower percentage of myelinated axons at the corpus callosum midline of 1 month-old cKO mice compared to controls (Fig. 3b and Supplementary Fig. 16) and a significantly increased *g*-ratio, a parameter often used to assess axonal myelination (Fig. 3c), indicating significantly reduced myelin thickness in cKO mice compared to controls. Similar myelination deficits were also observed in 2-week-old cKO mice compared to controls, although to a lesser extent (Supplementary Fig. 17). These myelination deficits persist in 6-month-old cKO mice compared to controls (Supplementary Fig. 18), suggesting they were not the result of delayed myelination.

To examine whether the myelination abnormalities found in cKO mice may lead to functional deficits, we measured the axonal conductivity of the corpus callosum in 1-month-old mice. We stimulated the axonal bundle of the corpus callosum of one hemisphere and recorded the evoked field potentials in the other

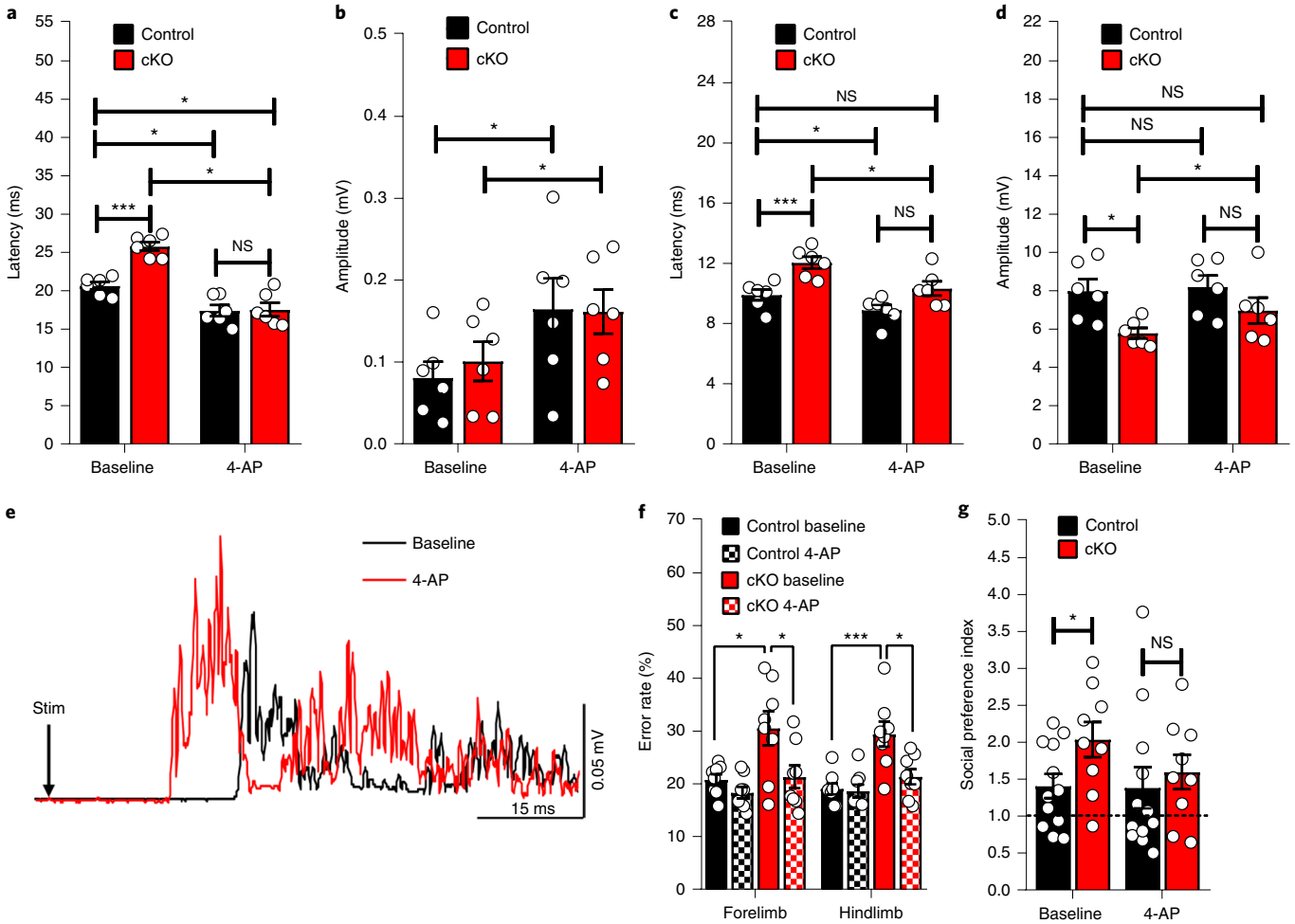

Fig. 4 | *Gtf2i* cKO mice impaired myelin-related properties are rescued following acute administration of 4-AP. a, Neuronal conductivity deficits in the CST of cKO mice, demonstrated by significantly longer response latency. Following acute administration of 4-AP, latency deficits are significantly decreased and normalized to control levels (control baseline versus cKO 4-AP $^{*}P=0.0411$; control baseline versus control 4-AP $^{*}P=0.0313$; cKO baseline versus cKO 4-AP $^{*}P=0.0313$; control baseline versus cKO baseline $^{***}P=0.0022$). **b**, Peak amplitude in the CST of cKO mice is not significantly different compared to controls, and it is increased following acute administration of 4-AP (control baseline versus control 4-AP $^{*}P=0.0313$; cKO baseline versus cKO 4-AP $^{*}P=0.0313$). **c**, Neuronal conductivity deficits in the corpus callosum of cKO mice, demonstrated by significantly longer response latency. Following acute administration of 4-AP, latency deficits are significantly decreased and normalized to control levels (control baseline versus control 4-AP $^{*}P=0.0313$; cKO baseline versus cKO 4-AP $^{*}P=0.0313$; control baseline versus cKO baseline $^{***}P=0.0043$). **d**, Peak amplitude in the corpus callosum of cKO mice is significantly lower compared to controls; it is increased following acute administration of 4-AP and normalized to control levels (cKO baseline versus cKO 4-AP $^{*}P=0.0313$; control baseline versus cKO baseline $^{*}P=0.0152$). **e**, Representative traces of evoked field potentials. **f**, The fine motor deficits in cKO mice are rescued following acute administration of 4-AP in both forelimb and hindlimb in the horizontal irregular ladder walking test (forelimb: control baseline versus cKO baseline $^{*}P=0.0127$, cKO baseline versus cKO 4-AP $^{*}P=0.0332$; hindlimb: control baseline versus cKO baseline $^{***}P=0.0013$, cKO baseline versus cKO 4-AP $^{*}P=0.011$). **g**, The social preference index, as measured in the three-chambered social test, was decreased and normalized to control levels in cKO mice following acute administration of 4-AP ($^{*}P=0.0365$). $^{*}P<0.05$, $^{**}P<0.01$, $^{***}P<0.005$. Two-tailed *t*-test (**a**–**d**,**f**–**g**). Data are shown as mean ± s.e.m. **a**–**d**, $n=6$ controls, $n=6$ cKO mice. **f**, $n=8$ controls, $n=8$ cKO mice. **g**, $n=12$ controls, $n=9$ cKO mice.

hemisphere. We found a significantly longer response latency (Fig. 3d) and significantly lower peak amplitude (Fig. 3e) of evoked field potentials in cKO mice compared to that of controls. However, no significant changes were found in the intrinsic membrane or firing properties of neurons in layer 5 of the primary motor cortex in *Gtf2i*-deleted neurons compared to controls (Supplementary Figs. 19 and 20).

Patients with WS demonstrate fine motor deficits and delays in the acquisition of early motor skills[2,28,29]. To investigate how deficits in myelination and axonal conduction might be affecting fine motor skills, mice were tested in the horizontal irregular ladder walking assay[30]. This test is known to be highly dependent on supraspinal connections composed of heavily myelinated long-distance axons[31]. Compared to controls, 1-month-old cKO mice showed a significant increase in the rate of imprecise paw placement in both forelimbs and hindlimbs (Fig. 3f,g). Additionally, forepaw and hindpaw grip strength was significantly reduced in cKO mice compared controls (Fig. 3h), indicating impaired descending drive to the motor neurons innervating the forepaws and hindpaws. In contrast, cKO mice showed no overt abnormalities in learning and executing the single pellet food retrieval task compared to controls (Fig. 3i). Thus, cKO mice showed impairments in the fine control of voluntary movements, along with weaker muscle tone for both forepaws and hindpaws, consistent with findings in patients with WS[2,29]. Notably, the axonal projection pattern of the corticospinal tract

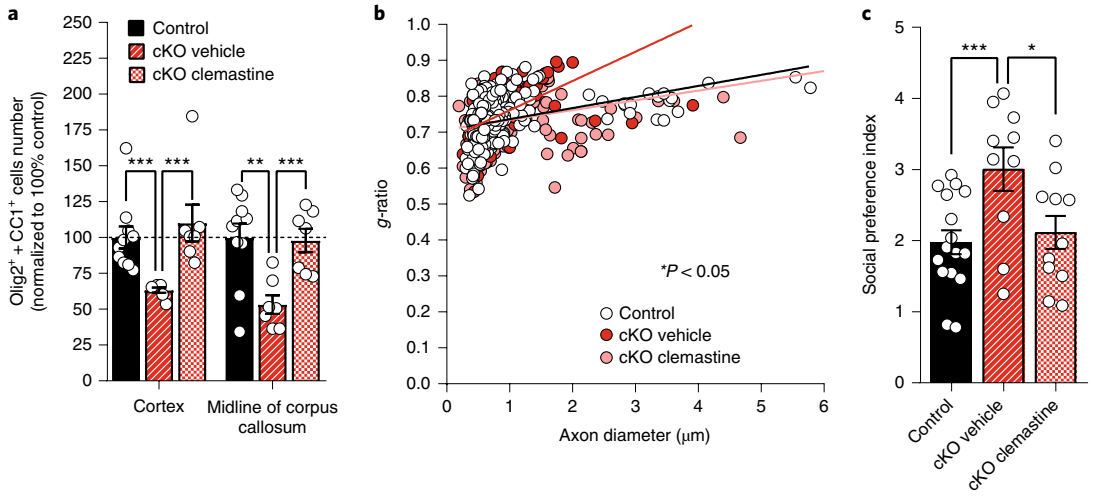

Fig. 5 | The impaired myelin-related properties of *Gtf2i* cKO mice are rescued following chronic administration of clemastine. a, After two weeks of clemastine administration, the number of oligodendrocytes in the cortex and midline of the corpus callosum of cKO mice was significantly increased and normalized to control levels (cortex: control versus cKO vehicle ***$P = 0.0001$, cKO vehicle versus cKO clemastine ***$P = 0.0006$; midline of corpus callosum: control versus cKO vehicle **$P = 0.0094$, cKO vehicle versus cKO clemastine ***$P = 0.0041$). **b**, Significantly increased myelin thickness in the midline of the corpus callosum of cKO mice following two weeks of clemastine administration, as measured by a significantly decreased *g*-ratio compared to cKO mice administered with vehicle only ($P = 0.0389$). **c**, Social preference index, as measured in the three-chambered social test, was decreased and normalized to control levels in cKO mice following two weeks of clemastine administration (control versus cKO vehicle ***$P = 0.0038$, cKO vehicle versus cKO clemastine *$P = 0.0301$). *$P < 0.05$, **$P < 0.01$, ***$P < 0.005$. **a**,**c**, Two-tailed *t*-test. **b**, One-way ANOVA with Dunnett's post hoc test. Data are shown as mean ± s.e.m. **a**, $n = 10$ controls, $n = 7$ cKO vehicle mice, $n = 7$ cKO clemastine mice. **b**, $n = 246$ axons from 3 control mice, $n = 281$ axons from 3 cKO vehicle mice, $n = 419$ axons from 4 cKO clemastine mice. **c**, $n = 16$ controls, $n = 10$ cKO vehicle mice, $n = 11$ cKO clemastine mice.

(CST) was unaffected by *Gtf2i* deletion, as indicated by similar corticospinal axon projection patterns and densities in the dorsal and intermediate laminae at the cervical and lumbar spinal cord levels (Supplementary Fig. 21).

To further characterize the physiological properties of these fine motor deficits, we measured functional connectivity in corticospinal output, by applying electrical stimulation in the primary motor cortex and recording electromyography (EMG) activity in the contralateral tibialis anterior muscle of the hindlimb. In cKO mice, the response latency of the EMG was significantly longer than in control mice (Fig. 4a, baseline), while EMG amplitude was similar to controls (Fig. 4b, baseline).

Normalization of impaired myelination properties or axonal conductivity rescues behavioral deficits. To investigate whether increasing axonal conductivity can rescue behavioral defects, we tested 4-aminopyridine (4-AP), a Food and Drug Administration (FDA)-approved medication that can improve axon conductivity by selectively blocking potassium channels[32]. Notably, the acute administration of 4-AP significantly shortened EMG latency in cKO and control mice, resulting in similar EMG latency of cKO and control mice (Fig. 4a, 4-AP). The EMG amplitudes of both control and cKO mice also increased significantly after 4-AP treatment (Fig. 4b, 4-AP). In addition, in the corpus callosum 4-AP treatment also normalized both the latency (Fig. 4c) and amplitude (Fig. 4d) of evoked potentials in cKO mice (Fig. 4e). Behaviorally, acute administration of 4-AP led to normalized fine motor skills in cKO mice in the horizontal irregular ladder walking test in both forelimb and hindlimb (Fig. 4f). Additionally, cKO mice showed normalized social preference following acute administration of 4-AP in the social preference test (Fig. 4g and Supplementary Fig. 22A,B).

To directly test whether changes in myelination led to the abnormal social behavior in cKO mice, we administrated the FDA-approved pro-differentiation compound clemastine to 1-month-old cKO mice for 2 weeks. Chronic clemastine treatment has been shown to promote oligodendrocyte differentiation and increase myelination[26,33–36]. We found that clemastine treatment normalized the number of oligodendrocytes in the cortex and the corpus callosum of cKO mice (Fig. 5a), and increased myelin thickness in cKO mice, as demonstrated by a significantly reduced *g*-ratio in cKO mice treated with clemastine compared to cKO mice administered with vehicle (Fig. 5b). Rescuing the myelination deficit was sufficient to normalize the social preference index in the social preference test (Fig. 5c and Supplementary Fig. 22C).

***Gtf2i*-Het mice demonstrate myelination-related deficits.** To examine whether the myelination deficits we found in cKO mice are present in *Gtf2i*-Het mice, which models the *Gtf2i* hemizygous human genetic condition in patients with WS, we also studied 1-month-old *Gtf2i* heterozygous mice. *Gtf2i* heterozygous mice (Supplementary Fig. 23A) showed significantly increased levels of anxiety-like behavior (Supplementary Fig. 23B) and social preference (Supplementary Fig. 23C,D), similar to cKO mice. Importantly, like cKO mice, *Gtf2i* heterozygous mice had significantly lower mRNA levels of myelin-related genes (Supplementary Fig. 23E) and significantly thinner myelin thickness compared to wild-type, as demonstrated by a significantly higher *g*-ratio (Supplementary Fig. 23F,G). Similar to cKO mice, no significant changes in passive and active membrane properties were found in neurons with *Gtf2i* hemizygosity, compared to controls (Supplementary Fig. 24).

Myelination-related transcriptomic, cellular and ultrastructural alterations in the frontal cortex of patients with WS. Moreover, to examine whether our findings of myelination deficits from mouse studies also present in patients with WS, we first ran RNA-Seq on frontal cortex samples from adult patients with WS with typical full WSCR deletion and normal controls (Fig. 6a and Supplementary Table 2). Although full WSCR deletion includes 26 genes, we found that 19% of all genes with significantly altered (increased or decreased) mRNA levels in patients with WS compared to controls are myelination-related genes (Fig. 6b,c and Supplementary Table 2). These genes had

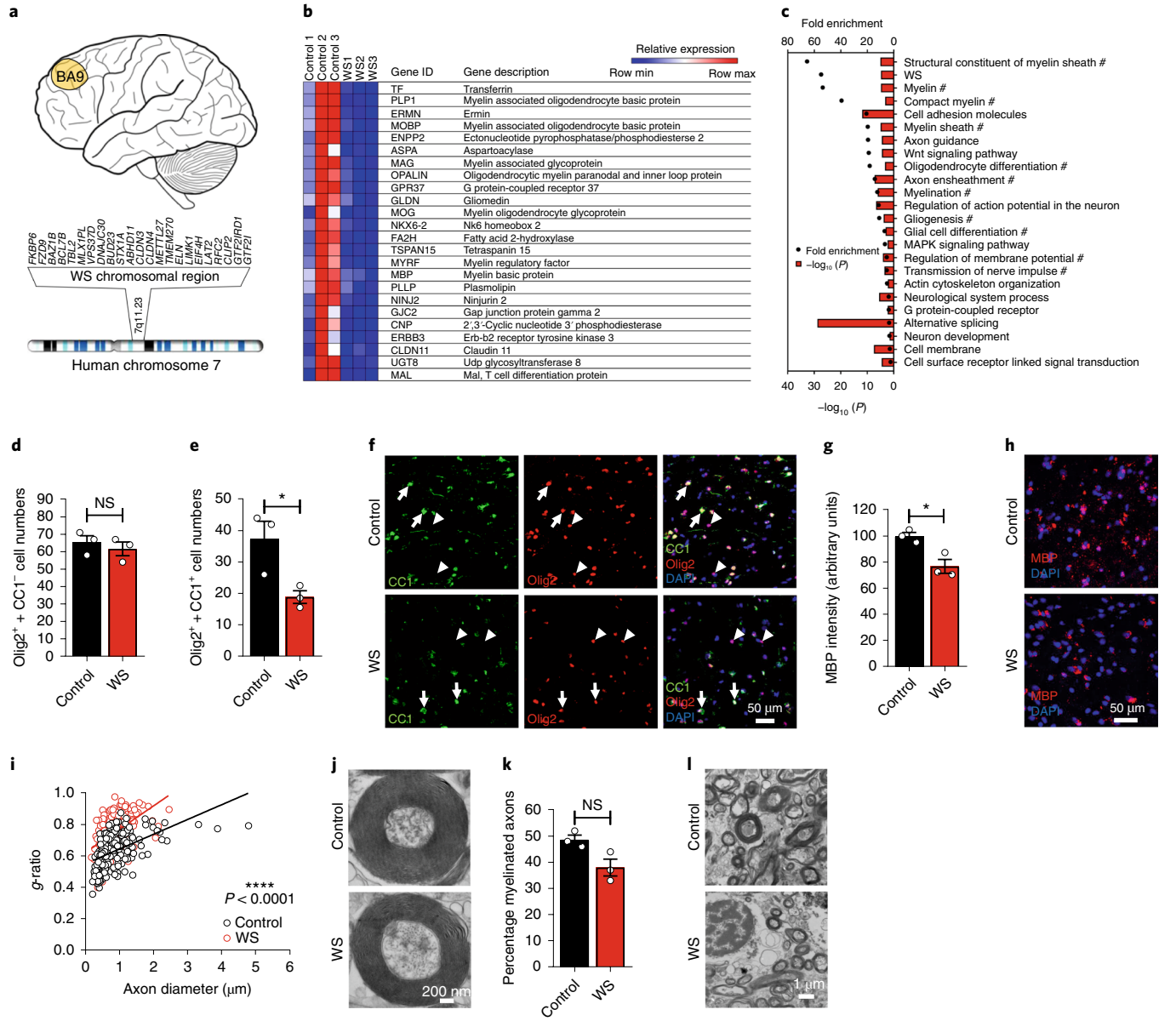

Fig. 6 | Myelination-related transcriptomic alterations in the frontal cortex of patients with WS. a, Diagram of the BA9 frontal cortical region of the human brain (top) and illustration of the WS chromosomal region (bottom). **b**, Gene expression heatmap table with all the myelination-related genes that had significantly decreased mRNA levels in patients with WS compared to typically developed controls. Genes that had significantly decreased mRNA levels also in *Gtf2i* cKO mice compared to controls are shown in bold. **c**, Significantly downregulated cellular pathways in patients with WS compared to typically developed controls, including myelination-related pathways (labeled with a hash (#) symbol). MAPK, mitogen-activated protein kinase. **d**, No significant difference in the number of $Olig2^+ + CC1^-$ cells in the cortex of patients with WS compared to controls ($P = 0.25$). **e**, The number of oligodendrocytes was significantly reduced in the cortex of patients with WS compared to controls ($P = 0.037$). **f**, Representative images of immunofluorescence labeling demonstrating reduced number of oligodendrocytes in the cortex of patients with WS compared to controls. This experiment was repeated independently in three pairs of human brain tissue with similar results. **g**, Significantly reduced intensity of myelin basic protein (MBP) in the cortex of patients with WS compared to controls ($P = 0.03$). **h**, Representative images of immunofluorescence labeling demonstrating reduced intensity of MBP in the cortex of patients with WS compared to controls. **i**,**j**, Significantly reduced myelin thickness in the frontal cortex of patients with WS (**j**), as measured by an increased *g*-ratio (**i**), in patients with WS compared to controls. **k**, A trend of lower percentage of myelinated axons in the frontal cortex of patients with WS compared to controls ($P = 0.057$). **l**, The myelin ultrastructure in human cortex. $^*P < 0.05$, $^{****}P < 0.0001$. **c**, Fisher's exact test. **d**,**e**,**g**,**i**,**k**, two-tailed *t*-test. Data are shown as mean ± s.e.m. **b**–**e**,**g**,**h**, $n = 3$ controls, $n = 3$ patients with WS. **i**, $n = 212$ axons from 4 controls, $n = 164$ axons from 3 patients with WS. **k**, $n = 4$ controls, $n = 3$ patients with WS.

significantly lower mRNA levels in patients with WS compared to controls (Fig. 6b,c); many of them are the same genes affected in *Gtf2i* cKO mice (in bold in Fig. 6b). In humans, these genes were significantly enriched in myelinating oligodendrocytes, as well as in premyelinating oligodendrocytes and OPCs, although to a lesser extent than in myelinating oligodendrocytes (Supplementary Fig.10, lower row). These genes encode proteins important for the formation, stability, compaction and maintenance of myelin[21–23]. Similar to the deficits characterized in cKO mice, we found no significant change in the number

of Olig2$^+$ + CC1$^-$ cells between patients with WS and controls (Fig. 6d), but significantly reduced oligodendrocyte numbers (Fig. 6e,f), and significantly reduced myelin basic protein (MBP) intensity (Fig. 6g,h) in the postmortem frontal cortex tissue of patients with WS compared to controls. Additionally, as in cKO mice, significantly decreased myelination thickness was found in patients with WS compared to controls, as indicated by a significantly increased *g*-ratio (Fig. 6i,j). Lastly, we found a trend of reduced percentage of myelinated axons in the postmortem frontal cortex tissue of patients with WS compared to controls (Fig. 6k,l, $P = 0.057$; $n = 4$ controls, $n = 3$ patients with WS).

Discussion

By deleting *Gtf2i* exclusively from excitatory neurons in mice, we unexpectedly found dramatic reduction in myelin-related gene transcripts, oligodendrocyte numbers, axon myelination and neuronal function. These results were further corroborated by similar transcriptional changes and myelination-related deficits in *Gtf2i* heterozygous deletion mice and in the brain of patients with WS. Together, these data suggest that myelination deficits are an important pathological change in WS; the deletion of *Gft2i* in WSCR is probably a cause of this pathology. Our study identified a previously unknown function of *Gtf2i* expression in excitatory neurons for proper oligodendrocyte development and myelination; this dysfunction may contribute to some of the neurological and behavioral symptoms associated with WS. This further supports the importance of axon–oligodendrocyte interaction in the development of myelination. Further study is needed to better understand the neurobiological mechanisms underlying signal transduction from excitatory neurons, regulated by TFII-I, to oligodendrocytes.

Previous human studies showed abnormalities in axonal integrity and myelination status in patients with WS[37–43]. These studies showed that radial diffusivity, an indicator of axonal integrity and myelination status, was significantly reduced in WS brains compared to controls[39]. However, the cellular nature of these deficits, and the molecular processes leading to them, were unknown. Our data are consistent with the clinical data and may provide a mechanistic explanation.

Previous mouse studies showed a relationship between white matter integrity and social behavior performance[44,45]. However, experimental evidence for this has been contrasting; for example, differences in both sensorimotor coordination and social interaction correlated with corpus callosum demyelination, demonstrated by an increased frequency of interactive behaviors among resident mice after acute or chronic demyelination by cuprizone[46]. On the other hand, mice given cuprizone for 28 d displayed fewer social interactions[47]; a positive correlation between corpus callosum thickness and social behavior was found[48]. Therefore, how myelination properties mediate social behavior developmentally and functionally in health or illness (that is, in WS), although of high interest, is largely unknown.

This study sheds light on how myelination and axonal conductivity properties affect social behavior in WS; therefore, it can facilitate the development of new treatment strategies for behavioral abnormalities. Because the efficiency and speed of conductivity relies on myelin[49], impairments in myelination might affect proper communication and synchronization between different brain regions essential for the correct execution of normal behaviors. Currently, the exact mechanisms underlying abnormal social behaviors in WS are not clear. Rescue of abnormal social behaviors in *Gtf2i*-mutant mice, by increasing axonal conductivity using 4-AP, suggests that the deficit is functional than structural/developmental. This is also consistent with recent studies showing rescue of social interaction deficits in adult mouse autism spectrum disorder models[50]. The improvement in social behaviors following clemastine treatment suggests that myelination-related deficits are responsible for behavioral alterations, and raises the possibility that targeting myelination deficits and their functional consequences might be a beneficial therapeutic strategy in WS.

Online content

Any methods, additional references, Nature Research reporting summaries, source data, extended data, supplementary information, acknowledgements, peer review information; details of author contributions and competing interests; and statements of data and code availability are available at https://doi.org/10.1038/s41593-019-0380-9.

Received: 21 November 2018; Accepted: 11 March 2019;
Published online: 22 April 2019

References

1. Barak, B. & Feng, G. Neurobiology of social behavior abnormalities in autism and Williams syndrome. *Nat. Neurosci.* **19**, 647–655 (2016).
2. Pober, B. R. Williams–Beuren syndrome. *N. Engl. J. Med.* **362**, 239–252 (2010).
3. Karmiloff-Smith, A. et al. Social cognition in Williams syndrome: genotype/phenotype insights from partial deletion patients. *Front. Psychol.* **3**, 168 (2012).
4. Dai, L. et al. Is it Williams syndrome? GTF2IRD1 implicated in visual-spatial construction and GTF2I in sociability revealed by high resolution arrays. *Am. J. Med. Genet. A* **149A**, 302–314 (2009).
5. Morris, C. A. et al. GTF2I hemizygosity implicated in mental retardation in Williams syndrome: genotype–phenotype analysis of five families with deletions in the Williams syndrome region. *Am. J. Med. Genet. A* **123A**, 45–59 (2003).
6. Bayés, M., Magano, L. F., Rivera, N., Flores, R. & Pérez Jurado, L. A. Mutational mechanisms of Williams–Beuren syndrome deletions. *Am. J. Hum. Genet.* **73**, 131–151 (2003).
7. Roy, A. L. Biochemistry and biology of the inducible multifunctional transcription factor TFII-I: 10 years later. *Gene* **492**, 32–41 (2012).
8. Osborne, L. R. Animal models of Williams syndrome. *Am. J. Med. Genet. C* **154C**, 209–219 (2010).
9. Segura-Puimedon, M. et al. Heterozygous deletion of the Williams–Beuren syndrome critical interval in mice recapitulates most features of the human disorder. *Hum. Mol. Genet.* **23**, 6481–6494 (2014).
10. Li, H. H. et al. Induced chromosome deletions cause hypersociability and other features of Williams–Beuren syndrome in mice. *EMBO Mol. Med.* **1**, 50–65 (2009).
11. Borralleras, C., Sahun, I., Pérez-Jurado, L. A. & Campuzano, V. Intracisternal *Gtf2i* gene therapy ameliorates deficits in cognition and synaptic plasticity of a mouse model of Williams–Beuren syndrome. *Mol. Ther.* **23**, 1691–1699 (2015).
12. Lucena, J. et al. Essential role of the N-terminal region of TFII-I in viability and behavior. *BMC Med. Genet.* **11**, 61 (2010).
13. Sakurai, T. et al. Haploinsufficiency of *Gtf2i*, a gene deleted in Williams Syndrome, leads to increases in social interactions. *Autism Res.* **4**, 28–39 (2011).
14. Enkhmandakh, B. et al. Essential functions of the Williams–Beuren syndrome-associated TFII-I genes in embryonic development. *Proc. Natl Acad. Sci. USA* **106**, 181–186 (2009).
15. Enkhmandakh, B. et al. Generation of a mouse model for a conditional inactivation of *Gtf2i* allele. *Genesis* **54**, 407–412 (2016).
16. Goebbels, S. et al. Genetic targeting of principal neurons in neocortex and hippocampus of NEX-Cre mice. *Genesis* **44**, 611–621 (2006).
17. Chailangkarn, T. et al. A human neurodevelopmental model for Williams syndrome. *Nature* **536**, 338–343 (2016).
18. Reiss, A. L. et al. An experiment of nature: brain anatomy parallels cognition and behavior in Williams syndrome. *J. Neurosci.* **24**, 5009–5015 (2004).
19. Thompson, P. M. et al. Abnormal cortical complexity and thickness profiles mapped in Williams syndrome. *J. Neurosci.* **25**, 4146–4158 (2005).
20. Cahoy, J. D. et al. A transcriptome database for astrocytes, neurons, and oligodendrocytes: a new resource for understanding brain development and function. *J. Neurosci.* **28**, 264–278 (2008).
21. Chang, K. J., Redmond, S. A. & Chan, J. R. Remodeling myelination: implications for mechanisms of neural plasticity. *Nat. Neurosci.* **19**, 190–197 (2016).
22. Rosenberg, S. S. & Chan, J. R. Modulating myelination: knowing when to say Wnt. *Genes Dev.* **23**, 1487–1493 (2009).
23. Rosenberg, S. S., Powell, B. L. & Chan, J. R. Receiving mixed signals: uncoupling oligodendrocyte differentiation and myelination. *Cell. Mol. Life Sci.* **64**, 3059–3068 (2007).

24. Nave, K. A. & Werner, H. B. Myelination of the nervous system: mechanisms and functions. *Annu. Rev. Cell Dev. Biol.* **30**, 503–533 (2014).
25. Liu, J. et al. Impaired adult myelination in the prefrontal cortex of socially isolated mice. *Nat. Neurosci.* **15**, 1621–1623 (2012).
26. Liu, J. et al. Clemastine enhances myelination in the prefrontal cortex and rescues behavioral changes in socially isolated mice. *J. Neurosci.* **36**, 957–962 (2016).
27. Liu, J. et al. Chromatin landscape defined by repressive histone methylation during oligodendrocyte differentiation. *J. Neurosci.* **35**, 352–365 (2015).
28. Chapman, C. A., du Plessis, A. & Pober, B. R. Neurologic findings in children and adults with Williams syndrome. *J. Child Neurol.* **11**, 63–65 (1996).
29. Trauner, D. A., Bellugi, U. & Chase, C. Neurologic features of Williams and Down syndromes. *Pediatr. Neurol.* **5**, 166–168 (1989).
30. Metz, G. A. & Whishaw, I. Q. Cortical and subcortical lesions impair skilled walking in the ladder rung walking test: a new task to evaluate fore- and hindlimb stepping, placing, and co-ordination. *J. Neurosci. Methods* **115**, 169–179 (2002).
31. Liu, Y. et al. A sensitized IGF1 treatment restores corticospinal axon-dependent functions. *Neuron* **95**, 817–833.e4 (2017).
32. Hayes, K. C. The use of 4-aminopyridine (fampridine) in demyelinating disorders. *CNS Drug Rev.* **10**, 295–316 (2004).
33. Green, A. J. et al. Clemastine fumarate as a remyelinating therapy for multiple sclerosis (ReBUILD): a randomised, controlled, double-blind, crossover trial. *Lancet* **390**, 2481–2489 (2017).
34. Cree, B. A. C. et al. Clemastine rescues myelination defects and promotes functional recovery in hypoxic brain injury. *Brain* **141**, 85–98 (2018).
35. Wang, F. et al. Enhancing oligodendrocyte myelination rescues synaptic loss and improves functional recovery after chronic hypoxia. *Neuron* **99**, 689–701.e5 (2018).
36. Mei, F. et al. Micropillar arrays as a high-throughput screening platform for therapeutics in multiple sclerosis. *Nat. Med.* **20**, 954–960 (2014).
37. Arlinghaus, L. R., Thornton-Wells, T. A., Dykens, E. M. & Anderson, A. W. Alterations in diffusion properties of white matter in Williams syndrome. *Magn. Reson. Imaging* **29**, 1165–1174 (2011).
38. Avery, S. N., Thornton-Wells, T. A., Anderson, A. W. & Blackford, J. U. White matter integrity deficits in prefrontal-amygdala pathways in Williams syndrome. *Neuroimage* **59**, 887–894 (2012).
39. Faria, A. V. et al. Quantitative analysis of gray and white matter in Williams syndrome. *Neuroreport* **23**, 283–289 (2012).
40. Hoeft, F. et al. More is not always better: increased fractional anisotropy of superior longitudinal fasciculus associated with poor visuospatial abilities in Williams syndrome. *J. Neurosci.* **27**, 11960–11965 (2007).
41. Jabbi, M. et al. The Williams syndrome chromosome 7q11.23 hemideletion confers hypersocial, anxious personality coupled with altered insula structure and function. *Proc. Natl Acad. Sci. USA* **109**, E860–E866 (2012).
42. Marenco, S. et al. Genetic contributions to white matter architecture revealed by diffusion tensor imaging in Williams syndrome. *Proc. Natl Acad. Sci. USA* **104**, 15117–15122 (2007).
43. Meyer-Lindenberg, A. et al. Neural correlates of genetically abnormal social cognition in Williams syndrome. *Nat. Neurosci.* **8**, 991–993 (2005).
44. Makinodan, M., Rosen, K. M., Ito, S. & Corfas, G. A critical period for social experience-dependent oligodendrocyte maturation and myelination. *Science* **337**, 1357–1360 (2012).
45. Miller, V. M. et al. Novel inter-hemispheric white matter connectivity in the BTBR mouse model of autism. *Brain Res.* **1513**, 26–33 (2013).
46. Hibbits, N., Pannu, R., Wu, T. J. & Armstrong, R. C. Cuprizone demyelination of the corpus callosum in mice correlates with altered social interaction and impaired bilateral sensorimotor coordination. *ASN Neuro* **1**, e00013 (2009).
47. Xu, H., Yang, H. J., McConomy, B., Browning, R. & Li, X. M. Behavioral and neurobiological changes in C57BL/6 mouse exposed to cuprizone: effects of antipsychotics. *Front. Behav. Neurosci.* **4**, 8 (2010).
48. Fairless, A. H. et al. Low sociability is associated with reduced size of the corpus callosum in the BALB/cJ inbred mouse strain. *Brain Res.* **1230**, 211–217 (2008).
49. Seidl, A. H. Regulation of conduction time along axons. *Neuroscience* **276**, 126–134 (2014).
50. Paul, L. K. et al. Agenesis of the corpus callosum: genetic, developmental and functional aspects of connectivity. *Nat. Rev. Neurosci.* **8**, 287–299 (2007).

Acknowledgements

The authors gratefully acknowledge M.E. Greenberg for advice and guidance and E. Okun, P. Monteiro, A. Krol, J. Wilde, A. Marco and S. Alon for insightful comments on the manuscript. H. Zaniewski and J. Wang provided technical help. Human tissue was obtained from the NIH NeuroBioBank at the University of Maryland. We thank the donors of the brain tissue and their families for their invaluable donations for the advancement of scientific understanding. This work is supported by a grant from the Simons Foundation (grant no. SFARI 240005 to G.F.), the Tang-Yang Center for Autism Research at MIT, the Poitras Center for Psychiatric Disorders Research at MIT, the Stanley Center for Psychiatric Research at Broad Institute of MIT and Harvard and the Simons Center for the Social Brain at MIT. B.B. was supported by postdoctoral fellowships from the Simons Center for the Social Brain at MIT and the Autism Science Foundation.

Authors contributions

B.B., Z.Z., Y.Liu., Z.H. and G.F. designed the experiments and wrote the manuscript. B.B. collected, analyzed and interpreted the results from studies related to behavior, biochemistry, genomics, immunofluorescence and pharmacology. M.E. collected and analyzed the results of immunofluorescence studies. Z.Z. collected, analyzed and interpreted the results from electrophysiological studies from the CST and corpus callosum. K.Q. collected, analyzed and interpreted the results from electrophysiological studies to characterize the properties of the basal membrane. K.M.L. collected and analyzed the results from the human immunostaining studies. Y.Liu collected, analyzed and interpreted the results from the fine motor skills and CST immunostaining studies. S.S.T. and A.N. collected, analyzed and interpreted the results from the clemastine study and the human immunofluorescence studies. D.W. administered the clemastine. Y.Li collected and analyzed the CST immunostaining studies. D.B. donated the *Gtf2i loxP* mice. B.B., G.L.B., Z.Z., Y.Liu, Z.H. and G.F. interpreted the results.

Competing interests

The authors declare no competing interests.

Additional information

Supplementary information is available for this paper at https://doi.org/10.1038/s41593-019-0380-9.

Reprints and permissions information is available at www.nature.com/reprints.

Correspondence and requests for materials should be addressed to B.B., Z.H. or G.F.

Publisher's note: Springer Nature remains neutral with regard to jurisdictional claims in published maps and institutional affiliations.

Methods

Mice. *Gtf2i loxP* mice[15] were backcrossed to pure C57Bl/6J (stock no. 000664; The Jackson Laboratory) for more than 15 generations. Germline deletion of a single *Gtf2i* allele (*Gtf2i*-Het mice) was achieved by breeding *Gtf2i loxP* mice to β-actin-cre transgenic mice, followed by another breeding to C57Bl/6J, to breed out the β-actin-cre. All animal-related work was performed under the guidelines of the Division of Comparative Medicine, with the protocol approved by the Committee for Animal Care of the Massachusetts Institute of Technology, and was consistent with the Guide for Care and Use of Laboratory Animals (1996 edition). Each cage contained 2–5 mice regardless of genotype; mice were housed at a constant 23 °C in a 12-h light–dark cycle (lights on at 7:00, lights off at 19:00) with ad libitum food and water. NEX-Cre mice are in a C57Bl/6 background[16]. NEX-Cre mice were previously shown to behave and develop normally, and to have Cre activity starting from around E11.5, specifically restricted to the excitatory neurons of the forebrain, located mainly in the cortex and hippocampus[16]. Rosa26-*loxP*-STOP-tdTomato$^{+/-}$ mice were used to assess Cre recombinase activity in the brain of 1-month-old male NEX-Cre mice.

Western blot. The whole cortex of 1-month-old mice was dissected and separated using SDS–polyacrylamide gel electrophoresis. The western blot was quantified using an Odyssey CLx imaging system (LI-COR). Commercial antibodies used include TFII-I (1:1,000; catalog no. 4562; Cell Signaling Technology) and monoclonal anti-α-tubulin (1:10,000; catalog no. T5168; Sigma-Aldrich), used as a loading control.

Behavioral studies. All behavioral studies were carried out and analyzed with the experimenter blinded to the genotypes. All test mice were males and were habituated in the test room for 1 h before all tests. Each cohort of test mice was used for a maximum of three behavioral tests with a minimum of 3 days break between tests. In all behavioral tests, except for the juvenile dyadic social interaction test, mice were 1 month old.

Juvenile dyadic social interaction test. The juvenile play apparatus was made of a non-transparent Plexiglas box (32 cm long × 32 cm wide × 32 cm high) and indirectly illuminated at 10 lx. Test mice were weaned at postnatal day 21 (P21) and individually habituated inside the test chamber with a thin layer of bedding for two consecutive days (two 30-min sessions per day). A pair of P23 test mice unfamiliar with each other and of the same genotype was gently placed into the test chamber and videorecorded for 10 min. Dyadic social interactions were scored with the Observer XT 12 software (Noldus Information Technology) by trained observers blinded to the genotypes. The following behaviors were coded: direct contact; following; nose-to-nose; nose-to-anogenital; crawling under or over; and allogrooming.

Social preference test. Stranger mice were wild-type S129 Sv males (The Jackson Laboratory) with age and body weight matched to the test mice. Stranger mice were habituated by placing them inside an inverted wire cup for 30 min (2 sessions per day for 3 consecutive days) before the tests. Each stranger mouse was used a maximum of two times per day. The social test apparatus was made of a clear Plexiglas box (65 cm long × 44 cm wide × 30 cm high) with a removable floor and partitions dividing the box into left, center and right chambers. The center chamber (21 × 22 cm) was half the width of the left and right chambers (each 21 × 44 cm^2). These three chambers were interconnected, with 5 cm openings between each chamber that could be opened or closed manually with a lever-operated door. The inverted wire cups containing the stranger mice were cylindrical, 10 cm high, with a bottom diameter of 10 cm and with metal bars spaced 0.8 cm apart. A weighted cup was placed on top of the inverted wire cup to prevent the test mice from climbing onto the wire cup. Each wire cup was used only once per day, followed by extensive cleaning with 75% ethanol and water at the end of the test day. During the habituation phase, an empty wire cup was placed into the left and right chambers, and each test mouse was placed into the middle chamber and allowed to explore for 15 min, with the doors into both side chambers left open. To test for social preference, the test mouse was gently introduced to the middle chamber with the doors to both side chambers closed; a stranger mouse was placed under the inverted wire cup in one of the side chambers and an inanimate object was placed under the inverted wire cup placed in the opposite side chamber. The location of the stranger mouse and object was counterbalanced between test trials to exclude side preference. The experimenter then lifted up the doorways to both side chambers simultaneously, and the test mouse was allowed to explore all three chambers for 15 min. Then, the experimenter blinded to the genotypes analyzed the time spent in close proximity to the stranger mouse or object using the EthoVision XT 13 software (Noldus Information Technology). The social preference index was calculated as follows: (time in close interaction with stranger mouse)/(time in close interaction with inanimate object).

Tube test. Transparent Plexiglas tubes (30 cm long and with a 3 cm inner diameter) were used so that 1-month-old mice could walk through without being able to reverse direction. Before testing, mice were habituated to walk through the tube two sessions per day for four consecutive days. On the test day, two unfamiliar mice with different genotypes were placed into the tube and released simultaneously by an experimenter blinded to their genotypes. The first mouse to completely retreat from the tube within the first 6 min of the test was defined as the loser; the other mouse was the winner. When no mice retreated within 6 min, tests were repeated with the entry sides reversed. The tubes were cleaned with 75% ethanol between trials. A chi-squared test was applied to determine the significance of the test score between mice when compared with an outcome expected by chance (that is, a 50:50 win–lose outcome).

Open field exploration test. Spontaneous locomotion was measured by placing mouse in a Plexiglas box (40 cm long × 40 cm wide × 30 cm high) for 1 h. Motor activity was detected by infrared photobeam sensors in an automated Omnitech Digiscan apparatus (AccuScan Instruments) and analyzed with the VersaMax Animal Activity Monitoring System (AccuScan Instruments). The experimenter was blind to the genotypes.

Elevated zero maze. The zero maze was indirectly illuminated at 60 lx on the open arms and 10 lx on the closed arms. Testing started with a mouse being placed inside a closed arm of the maze. Behavior was videorecorded for 5 min. The experimenter was blind to the genotypes.

Hot plate. Mice were placed onto a heating block set to a 55 °C surface temperature (Columbus Instruments International). Latency to lick a forepaw or hindpaw was measured. An average of three trials, with an intertrial interval of 5 min, was recorded. The experimenter was blind to genotypes.

Acoustic startle response and prepulse inhibition test. The experiments were performed with two identical sound-attenuating test chambers (65 cm long × 35 cm wide × 25 cm high). Each test chamber was equipped with a loudspeaker mounted 25 cm above the holding cylinder and a commercial startle reflex system (SR Lab; San Diego Instruments). An individual mouse was placed inside the Plexiglas holding cylinder mounted on a Plexiglas platform. A piezoelectric accelerometer located beneath the platform was used to transform startle responses into units based on the force and latency of startle. Data were collected at 250 samples s^{-1}; the maximum voltage attained on each trial was used as the dependent variable. Each test session started with a 5 min acclimation period in the presence of 65 dB acoustic background noise followed by five 120 dB startle pulses. Prepulse trials followed the initial 120 dB startle acclimation. Each prepulse stimulation was 20 ms in duration, followed by a 40 ms startle stimulus of 120 dB. Prepulse inhibition was recorded for prepulse intensities of 70, 75, 80, 85 and 90 dB, and no stimulus. Each prepulse trial was administered ten times in a random order. Trials of 120 dB alone were randomly interspersed within the prepulse trials and used for comparison with the prepulse trials. The percentage prepulse inhibition was calculated using the formula (100−(response to prepulse + 120 dB)/(response for 120 dB alone) × 100). The acoustic startle trials followed the prepulse inhibition trials. The startle trials consisted of 40 ms pulses at 0 (no stimulus), 70, 75, 80, 85, 90, 95, 100, 105, 110, 115 and 120 dB. Each trial was presented five times in a randomized order. The experimenter was blind to the genotypes.

Horizontal irregular ladder walking. Mice were tested for their ability to walk on a horizontal ladder with irregularly spaced rungs, following the procedure described previously[30]. Animals were trained to cross the ladder until their performance achieved the plateau (forelimb error ≤ 20%). The irregular pattern was changed from trial to trial during training. All trials were videorecorded with HotShot e64 camera (nac Image Technology) and paw placement was analyzed. Paw placement on rungs was categorized as hit (plantar contact and digits closure), miss (paw falls between the rungs) and slip (imprecise contact with one or several digits). The experimenter was blind to the genotypes.

Grip strength. The grip strength of mice forelimbs and hindlimbs was measured using a Grip Strength Meter (TSE Systems) according to the manufacturer's instructions. Each mouse was tested on three consecutive trials to obtain the average force (*g*). The experimenter was blind to the genotypes.

Single pellet food retrieval task. The single pellet food retrieval task was carried out following previously established procedures with minor modifications[51]. Mice were placed into the clear Plexiglas training chamber (1 mm thick; dimensions 20 × 15 × 8.5 cm^3) with a narrow vertical slit (0.5 cm wide and 13 cm high) located on the front wall of the chamber. Single sugar pellet (dustless precision pellet, 20 mg; Bio-Serv) was placed on an exterior shelf affixed to the wall in front of the slit, at a height of 1.5 cm. Mice were food-restricted for 1 night before training and were maintained above 90% of free-feeding weight throughout the training session. Twenty pellets were used for daily training until the performance plateaued. The success rate was calculated as: number of successful retrievals/total attempts per trail × 100. The experimenter was blind to the genotypes.

RNA isolation and quantitative PCR (qPCR). For the human tissue samples, frozen tissue was used directly from −80 °C. For the mouse tissue, mice were decapitated after an isoflurane overdose and the whole cortex was dissected

and snap-frozen on dry ice. Total RNA was extracted using the RNeasy Mini kit (QIAGEN) according to the standard user manual. Equivalent amounts of mouse total mRNA were reverse-transcribed to complementary DNA with the iScript cDNA Synthesis Kit (Bio-Rad Laboratories). Real-time qPCR was carried out using the iQ5 real-time PCR detection system (Bio-Rad Laboratories) with the iQ SYBR Green Supermix Kit (Bio-Rad Laboratories) according to the manufacturer's protocol.

RNA-Seq analysis. For quality control purposes, bedtools v.2.17.0 was used to count the reads classified as genes, coding regions, intronic regions, 5′ or 3′ untranslated regions, flanking 3 kb genic regions and intergenic regions. Other basic statistics, including mapping rate, ratio of sense versus antisense reads and ribosomal RNA percentages, were collected for each sample. RSEM v.1.2.15 was used to estimate gene expression levels based on mm9 University of California Santa Cruz known gene annotations. The count table was imported into DESeq v.1.10.1 for differential gene expression testing. The gene expression ($\log_2$fragments per kilobase of transcript per million mapped reads (FPKM)) table was then run through Gene Set Enrichment Analysis (GSEA), which determines whether a set of genes defined a priori shows statistically significant, concordant differences between two biological states. To do functional analysis with DAVID (version 6.7), up- and downregulated coding genes ($P < 0.05$) were compared to the expressed genes (coding genes with an average FPKM > 1). Networks were also generated through the use of QIAGEN's Ingenuity Pathway Analysis (www.qiagen.com/ingenuity).

GSEA analysis. GSEA was performed to determine whether the myelination-related downregulated gene set from the mouse and human samples are enriched within OPCs, newly formed oligodendrocytes or myelinating oligodendrocytes (http://www.broad.mit.edu/gsea/).

Immunofluorescence staining. A basic immunofluorescence procedure was used as described previously[52]. Mice were deeply anesthetized with isoflurane and transcardially perfused with 15 ml ice-cold PBS solution followed by 15 ml fresh ice-cold 4% paraformaldehyde (PFA) in PBS. Brains were dissected and kept in 4% PFA overnight at 4 °C and then sectioned at a 100 µm thickness using a vibratome (Leica). Floating brain slices were washed 3 times, 5 min each, with PBS and permeabilized with 1.2% Triton X-100 in PBS for 15 min at room temperature. Slices were then washed 3 times, 5 min each, followed by blocking with 5% normal goat serum, 2% bovine serum albumin and 0.2% Triton X-100 in PBS for 1 h at room temperature. Primary antibodies diluted in blocking buffer were applied to sections overnight at 4 °C. Slices were then washed 3 times with PBS, 15 min each, and stained with secondary antibodies conjugated with Alexa Fluor 488, 555 and 647 (1:1,000; catalog nos. A-11094, A-21429 and A-21245; Thermo Fisher Scientific) in blocking buffer for 1 h at room temperature. Slices were washed twice in PBS for 15 min, followed by 4,6-diamidino-2-phenylindole (DAPI; 1:10,000) staining in PBS for 5 min, and an additional 5 min wash in PBS. VECTASHIELD Antifade Mounting Medium (Vector Laboratories) was used to mount the slices on glass slides. Images were captured using an FluoView FV1000 confocal microscope (Olympus).

To quantify the cellular properties in the cortex, images were taken by an experimenter blind to the genotypes with a ×10 magnification at the motor cortex area (bregma 0.5 mm). For each mouse, both hemispheres were imaged. The midline of the corpus callosum was imaged at the same bregma, using a ×40 magnification; the whole depth of the corpus callosum was imaged by taking 10 images as part of a z-stack serial imaging. Then, all images were stacked together to a single image that was analyzed for quantification. Cell numbers were quantified blindly with automation using ImageJ (NIH). For the cortex, the two values of the hemispheres from each mouse were averaged. The pixel intensity of H3ac and H3K9me3 was quantified with ImageJ, as described previously[25].

Commercial antibodies used include: TFII-I; anti-CaM Kinase IIa, α subunit, clone 6G9 (1:400; catalog no. 05-532; EMD Millipore); GFP (1:3,000; A11122; Invitrogen); Sox-10 (1:100; catalog no. sc-365692; Santa-Cruz Biotechnology); PDGFR-α (1:1,000; catalog no. sc-338; Santa-Cruz Biotechnology); Anti-Olig-2 (1:1,000; catalog no. AB9610; EMD Millipore); Anti-APC (Ab-7) (1:500; catalog no. OP80; Calbiochem); Anti-NeuN, clone A60 (1:1,000; catalog no. MAB377; EMD Millipore); anti-S-100 (β-Subunit) (1:600; catalog no. S2532; Sigma-Aldrich); and Anti-GAD67, clone 1G10.2 (1:1,000; catalog no. 5406; EMD Millipore).

E15.5 immunohistochemistry. Females mice were checked daily for semen plugs and separated from male mice once a plug was detected. Pregnant dams were killed on E15.5 and embryos were immediately dissected in ice-cold PBS. Tissue was taken for genotyping and brains were dissected and transferred to ice-cold 4% PFA. Whole brains were fixed in 4% PFA overnight, embedded in optimal cutting temperature compound and 12 µm coronal sections were cut using a cryostat (Leica).

Electron microscopy. One-month-old or 6-month-old mice were deeply anesthetized with isoflurane, transcardially perfused with 15 ml ice-cold PBS solution followed by 15 ml fresh ice-cold 2.5% glutaraldehyde + 2% PFA in 0.1 M sodium cacodylate buffer (pH 7.4). Brains were dissected and kept in the fixation solution overnight at 4 °C. Small pieces (1–2 mm cubes) of tissue samples from the corpus callosum at the level of the fornix were postfixed for at least 2 h at room temperature in the fixation solution, washed in 0.1 M sodium cacodylate buffer and postfixed with 1% osmium tetroxide/1.5% potassium ferrocyanide for 1 h, washed in water 3 times and incubated in 1% aqueous uranyl acetate for 1 hr followed by 2 washes in water and subsequent dehydration in grades of alcohol (10 min each; 50, 70, 90 and 2 × 10 min 100%). The samples were then put in propylene oxide for 1 h and infiltrated overnight in a 1:1 mixture of propylene oxide and epoxy resin mixture (TAAB Epon; Marivac Canada). The following day, samples were embedded in TAAB Epon and polymerized at 60 °C for 48 h. Ultrathin sections (approximately 60 nm) were cut on a Reichert Ultracut S microtome (Leica), picked up on copper grids stained with lead citrate and examined in a JEOL 1200EX transmission electron microscope (JEOL USA, Inc., USA) or a Tecnai G² Spirit BioTWIN (FEI Company, USA) and images were recorded with an 2k CCD camera (Advanced Microscopy Techniques). To quantify the number of myelinated axons and characterize the *g*-ratio, three images were taken along the dorsoventral axis of the corpus callosum in each of three different locations along the mediolateral axis of the corpus callosum, to cover multiple regions of the corpus callosum (Supplementary Fig. 25). To quantify the *g*-ratio, approximately 100–150 myelinated axons per mouse were analyzed by an experimenter blind to the genotypes, by manually measuring the ratio of the axon diameter and myelinated axon diameter. To quantify the percentage of myelinated axons in the corpus callosum, 1,500 axons per mouse were analyzed by an experimenter blind to the genotypes, by manually counting the myelinated and unmyelinated axons.

Nucleic heterochromatin was determined as described previously[25]. Briefly, oligodendrocyte cells were identified by an experimenter blind to the genotypes by the presence of microtubules combined with the absence of intermediate filaments and glycogen granules. The total nuclear area was calculated by isolating the nucleus of each cell using the 'clear outside' function of the ImageJ software. Heterochromatin, qualitatively defined as a gray scale density ≥ 100 on a 256 gray scale, was selected using the threshold tool and reported as the percentage of the total nuclear area.

For human samples, fixed tissue was used and processed similarly to mouse brain tissue. To quantify the *g*-ratio, approximately 100 myelinated axons per human participant were analyzed by an experimenter blind to the genotypes, by manually measuring the ratio of the axon diameter and myelinated axon diameter. To quantify the percentage of myelinated axons in the frontal cortex of humans, approximately 300 axons per individual were analyzed by an experimenter blind to the genotypes, by manually counting the myelinated and unmyelinated axons.

Evoked field potential recordings in the corpus callosum. The in vivo evoked field potential recordings in the corpus callosum were referenced to those from the in vitro studies[53,54]. Animals were anesthetized with urethane (1,000 mg kg^{-1}) and placed on a stereotaxic instrument. Body temperature was maintained by thermostat at 37.5–38 °C. Craniotomy was performed and the dura was intact. A stainless steel stimulation electrode (300–500 kΩ; World Precision Instruments) was positioned in the corpus callosum in the left hemisphere (1.5 mm posterior to bregma, 1 mm lateral from midline, 1,000–1,300 µm beneath the cortical surface); a tungsten recording electrode (2–3 MΩ; FHC) was positioned in the corpus callosum in the right hemisphere at the same coronal plane (1.5 mm posterior to bregma, 1 mm from midline, 1,000–1,300 µm beneath the cortical surface). Electrical stimulation (0–200 µA, 0.2 ms pulse width, 0.2 Hz) was delivered, while the positions of the stimulation and recording electrodes were slightly adjusted to optimize the signal. Signals were filtered at 0.1–3,000 Hz and gained at 1,000 times (Model 1700 Differential AC Amplifier; A-M Systems), digitized and sampled at 10,000 Hz (Digidata 1440A; Molecular Devices), and analyzed offline (Clampfit software 10). Electrical stimulation was increased from 0 µA with 10 µA steps until response latency reached minimum and response amplitude reached maximum. Peak latency was defined as time from stimulation onset to response peak. Response amplitude was determined by measuring the vertical distance from the negative peak to the tangent joining the preceding and following positivities. After recording, a 10 µA constant current for 10 s was delivered at all electrodes to burn small holes at the tips; fluorescent Nissl staining was performed on perfused brain slices to verify that the electrodes were in the desired position. The experimenter was blind to the genotypes.

4-AP pharmacological treatment. Mice were habituated to needle injections (intraperitoneal) for 3 d before the behavioral tests, by 2 intraperitoneal injections of 200 µl saline administered per day. Based on the calibration experiments we ran, we found that 4-AP (1 mg kg^{-1}; catalog no. 275875; Sigma-Aldrich) achieved its maximal effect within 1–3 h post-systemic intraperitoneal administration. Therefore, all behavioral tests were accomplished 3 h post-systemic administration. Saline-injected mice in each genotype (control or cKO mice) were the baseline group for the treatment group that was injected with 4-AP. The experimenter was blind to the genotypes.

Clemastine pharmacological treatment. For the chronic clemastine treatment, mice were given vehicle (dimethylsulfoxide (DMSO)) or clemastine (dissolved in

DMSO, 10 mg kg^{-1} body weight; Tocris Bioscience) daily through gastric gavage for 14 consecutive days before tests were undertaken. The experimenter was blind to the genotypes.

Corticospinal axon projection characterization. AAV2.8-ChR2-mCherry (titer: 1×10^{13} copies ml^{-1}) was unilaterally delivered to the sensorimotor cortex by stereotaxic brain injection[31]. Two weeks later, animals who had received the brain injection were perfused. Transverse sections of the spinal cord were then processed for immunostaining with primary antibody against red fluorescent protein (1:200; catalog no. ab34771; Abcam). Images were taken with an LSM 700 confocal microscope (ZEISS). ImageJ was used to quantify the fluorescence intensities. The experimenter was blind to the genotypes.

Intracortical microstimulation and EMG recording. The intracortical microstimulation and EMG recording protocol was adopted from previous studies[55,56]. Animals were anesthetized with ketamine–xylazine (100 mg kg^{-1} ketamine, 10 mg kg^{-1} xylazine, administered intraperitoneally). Anesthesia was maintained at a steady level such that the animal was unresponsive to toe pinching while muscle tone was present. Supplemental doses of ketamine–xylazine at one tenth of the initial dose were administrated every 30 min or when the breathing rate dramatically increased and whiskers started to shake.

A digital stereotaxic frame was used to mount the animal's head and guide the stimulation electrode (stainless steel, 0.5 MΩ; World Precision Instruments) over an array of motor cortical sites (0.9 mm caudal and 0.6 mm rostral to bregma, 0.9–1.8 mm lateral to midline, with 300 µm spacing between sites). The stimulation electrode was inserted into the cortex at 500 µm depth, targeting layer V motor neurons. The exposed brain area was immersed in silicon oil to avoid dehydration. Electrical stimulation (biphasic, 0.2 ms pulse width, 333 Hz, 45 ms) was adjusted between 100 and 300 µA and located at the position with the lowest threshold to trigger the EMG signal. Stimulation intensity of twofold the threshold was then used for EMG recording and analysis. To perform the EMG recording, an incision was made on the hindlimb to expose the muscles while the fascia remained intact. Nichrome wires (catalog no. 762000; A-M Systems) were deinsulated at the tip for 1 mm and customized for a small hook that secures the position within the muscle. A pair of electrodes were then inserted into the motor end plate area of tibialis anterior muscle using a 25 G needle. The EMG signals were acquired using a differential AC amplifier (Model 1700; A-M Systems) with a 10–1,000 Hz bandpass filter, sampled at 5 kHz using a digitizer (Digidata 1440A; Molecular Devices) and analyzed with the pCLAMP 10 software. The EMG traces were rectified and averaged among traces; the peak amplitude in a window of 0–50 ms from stimulation onset was used to define the EMG response. Latency was defined by measuring the time from stimulation onset to the beginning of the EMG response over 3 times the standard deviation of baseline.

4-AP (2 mg kg^{-1}) was administrated intraperitoneally; a post-treatment test was carried out 30–60 min after the injection. The experimenter was blind to the genotypes.

Slice physiology. Mice were deeply anesthetized with isoflurane, then perfused with ice-cold, oxygenated sucrose cutting solution (30 mM NaCl, 4.5 mM KCl, 1.2 mM NaH_2PO_4, 26 mM $NaHCO_3$, 194 mM sucrose, 10 mM glucose, 8 mM $MgCl_2$, 0.2 mM $CaCl_2$). The brain was dissected and 300 µm thick coronal slices of M1 were sectioned on a vibratome (VT1200; Leica) in the sucrose cutting solution. Slices were recovered in oxygenated artificial cerebrospinal fluid (119 mM NaCl, 11 mM glucose, 26.2 mM $NaHCO_3$, 2.3 mM KCl, 2.5 mM $CaCl_2$, 1 mM NaH_2PO_4 and 1.3 mM $MgCl_2$, pH 7.3, 310–320 mOsm) at 37 °C for 8 min and allowed to acclimate to room temperature for at least 30 min before recordings were made.

Intrinsic membrane and spiking properties were recorded from layer V M1 pyramidal cells in oxygenated artificial cerebrospinal fluid using an internal solution that contained (120 mM potassium gluconate, 10 mM KCl, 10 mM phosphocreatine, 4 mM Mg-ATP, 0.3 mM Na-GTP, 10 mM HEPES and 0.1% biocytin, pH 7.3, 290–300 mOsm). The resting potential and compensated input resistance were recorded within seconds of breaking into a cell. Cells with a series resistance < 25 MΩ and < 25% change for the duration of the experiment were used for analysis. Analysis of current-clamp electrophysiological data was performed with pCLAMP10 (Molecular Devices). The single action potential parameters (peak amplitude, half-width and hyperpolarization anti-peak) were measured at the threshold and spike amplitudes; the after-hyperpolarization potentials were measured relative to the spike threshold. To measure the pyramidal cell firing properties, the frequency–current relationship (*FI* curve) was calculated as the spike frequency after the current steps from 0 pA (resting approximately −60 mV) to 1,000 pA were applied in increments of 50 pA (0.05 Hz, 1,000 ms duration). The experimenter was blind to the genotypes.

Human samples. Human brain samples of the frontal cortex (Brodmann area 9 (BA9)) were obtained from the NIH NeuroBioBank at the University of Maryland. Frozen and fixed tissue from patients with WS and controls was used (Supplementary Table 3). All relevant ethical regulations were complied with. The NIH NeuroBioBank at the University of Maryland provided guidelines for study procedures.

Fluorescence in situ hybridization (FISH) on human tissue. Blocks of fresh-frozen control and WS human BA9 cortical brain samples were acquired from the NIH NeuroBioBank at the University of Maryland. Blocks were then embedded in optimal cutting temperature freezing medium and flash-frozen in an isopropyl alcohol/dry ice bath. Samples were cut on a cryostat (CM 850; Leica) into 16 µm sections, adhered to SuperFrost Plus adhesion slides (catalog no. 12-550-15; Thermo Fisher Scientific) and stored at −80 °C until use. Samples were immediately fixed in 4% PFA for 20 min on ice and stained on the slide according to the RNAscope Fluorescent Multiplex Assay (catalog no. 320850; Advanced Cell Diagnostics) protocol. Samples were stained for MBP (RNAscope Probe-Hs-MBP; catalog no. 411051; Advanced Cell Diagnostics) with antisense probes and coverslipped with VECTASHIELD Hardset Antifade Mounting Medium with DAPI (catalog no. H-1500; Vector Laboratories). Z-stack serial images were taken through the whole depth of the field on an Eclipse Ti inverted microscope (Nikon Instruments) with an Andor CSU-W1 confocal spinning disc unit and an Andor DU-888 EMCCD camera using a ×20, 0.75 numerical aperture (NA) air objective and a ×60, 1.40 NA oil immersion objective. Fields of view were randomly chosen across the whole cortical sample. The Experimenter was blind to the genotypes.

FISH analysis and quantification. Quantification of colocalization and fluorescence intensity was performed on ×20 images using the Cell Counter Fiji ImageJ plugin and was performed blinded to sample type. For quantification purposes, all image z-stacks were max-projected, adjusted for brightness and contrast, and color flattened identically across samples using ImageJ. The *PDGFRA* FISH experiments were quantified per cell, identified by DAPI, per 1,024 × 1,024 pixel field of view, taken from two adjacent fields of view stitched together. The *MBP* FISH experiments were analyzed for the corrected total cell fluorescence to match the quantification from the immunofluorescence staining procedures as described previously; 400 × 400 pixel random fields of view were used to calculate the corrected total cell fluorescence levels of *MBP* in ImageJ. The experimenter was blind to the genotypes.

Human tissue immunofluorescence. Blocks of fresh-frozen control and WS human BA9 cortical brain samples were acquired from the NIH NeuroBioBank at the University of Maryland. Blocks were then embedded in optimal cutting temperature freezing medium and flash-frozen in an isopropyl alcohol/dry ice bath. Samples were cut on a CM 850 cryostat into 16 µm sections, adhered to SuperFrost Plus adhesion slides and stored at −80 °C until use. Sections were air-dried for 20 min at room temperature before being fixed in 4% PFA for 30 min at 4 °C. Samples were washed, then permeabilized and blocked with 1.2% Triton X-100 and 3% normal goat serum in PBS at room temperature for 1 h, before being incubated for 5 d at 4 °C with the primary antibodies Anti-Olig-2 and Anti-APC (1:2). Samples were washed extensively in PBS and then stained with secondary antibodies conjugated with Alexa Fluor 488 and 568 for 2 h at room temperature (1:500; catalog nos. A-11001 and A-21429; Thermo Fisher Scientific). As a final step, TrueBlack Lipofuscin Autofluorescence Quencher (catalog no. 23007; Biotium) was incubated on the samples for 1.5 min at room temperature in 70% ethanol and then washed thoroughly in PBS, before staining with DAPI, and then coverslipped with VECTASHIELD Antifade Mounting Medium. Images were taken on a Fluoview FV1000 confocal microscope, using a ×20, 0.75 NA objective, and on an Olympus BX61 Epi microscope (Olympus), using a ×10, 0.40 NA objective.

To quantify the results, images were taken with the same imaging constraints and corrections. Cell numbers were quantified blindly by an experimenter, who counted the number of $Olig2^+$ $CC1^+$ cells.

Statistical analysis. All comparisons between groups were collected from littermate animals with experiments performed at the same time. All datasets were analyzed using the D'Agostino–Pearson omnibus test or Shapiro–Wilk test for normality. Datasets with normal distributions were analyzed for significance using either unpaired two-tailed Student's *t*-tests or one-way or two-way analysis of variance (ANOVAs) with proper post-hoc test (Prism 8; GraphPad Software). Datasets with non-normal distributions were analyzed using a Kruskal–Wallis test with adjustments for multiple comparisons or Wilcoxon signed-rank test. Further details on particular statistical analyses can be found on the respective figures/results section for each dataset. No statistical methods were used to predetermine sample size, but our sample sizes are similar to those reported in previous publications[10,11,13,25]. No animal or sample was excluded from the analysis. Experiments were randomized (mice order, items' positions and sample loading were all randomized and counterbalanced) and the investigators were blind to the genotypes during the experiments and outcome assessment. All results were presented as the mean ± s.e.m.

Reporting Summary. Further information on research design is available in the Nature Research Reporting Summary linked to this article.

Data availability

All data are available in the main text or the supplementary materials. All RNA-Seq datasets generated and analyzed during the current study are available in the supplementary tables and from the corresponding author upon reasonable request. RNA data are available in the Gene Expression Omnibus (GEO) with accession

code GSE128841. All data generated in this study are deposited in the GEO under accession code TBD.

References

51. Blanco, J. E., Anderson, K. D. & Steward, O. Recovery of forepaw gripping ability and reorganization of cortical motor control following cervical spinal cord injuries in mice. *Exp. Neurol.* **203**, 333–348 (2007).
52. Barak, B. et al. Neuron-specific expression of tomosyn1 in the mouse hippocampal dentate gyrus impairs spatial learning and memory. *Neuromolecular Med.* **15**, 351–363 (2013).
53. Crawford, D. K. et al. Oestrogen receptor β ligand: a novel treatment to enhance endogenous functional remyelination. *Brain* **133**, 2999–3016 (2010).
54. Crawford, D. K., Mangiardi, M. & Tiwari-Woodruff, S. K. Assaying the functional effects of demyelination and remyelination: revisiting field potential recordings. *J. Neurosci. Methods* **182**, 25–33 (2009).
55. Asante, C. O. & Martin, J. H. Differential joint-specific corticospinal tract projections within the cervical enlargement. *PLoS One* **8**, e74454 (2013).
56. Wang, X. et al. Deconstruction of corticospinal circuits for goal-directed motor skills. *Cell* **171**, 440–455.e14 (2017).

Corresponding author(s): Guoping Feng
Zhigang He
Boaz Barak

Last updated by author(s): 2019/02/04

Reporting Summary

Nature Research wishes to improve the reproducibility of the work that we publish. This form provides structure for consistency and transparency in reporting. For further information on Nature Research policies, see Authors & Referees and the Editorial Policy Checklist.

Statistics

For all statistical analyses, confirm that the following items are present in the figure legend, table legend, main text, or Methods section.

n/a	Confirmed	
☐	☒	The exact sample size (*n*) for each experimental group/condition, given as a discrete number and unit of measurement
☐	☒	A statement on whether measurements were taken from distinct samples or whether the same sample was measured repeatedly
☐	☒	The statistical test(s) used AND whether they are one- or two-sided *Only common tests should be described solely by name; describe more complex techniques in the Methods section.*
☐	☒	A description of all covariates tested
☐	☒	A description of any assumptions or corrections, such as tests of normality and adjustment for multiple comparisons
☐	☒	A full description of the statistical parameters including central tendency (e.g. means) or other basic estimates (e.g. regression coefficient) AND variation (e.g. standard deviation) or associated estimates of uncertainty (e.g. confidence intervals)
☐	☒	For null hypothesis testing, the test statistic (e.g. *F*, *t*, *r*) with confidence intervals, effect sizes, degrees of freedom and *P* value noted *Give P values as exact values whenever suitable.*
☐	☒	For Bayesian analysis, information on the choice of priors and Markov chain Monte Carlo settings
☐	☒	For hierarchical and complex designs, identification of the appropriate level for tests and full reporting of outcomes
☐	☒	Estimates of effect sizes (e.g. Cohen's *d*, Pearson's *r*), indicating how they were calculated

Our web collection on statistics for biologists contains articles on many of the points above.

Software and code

Policy information about availability of computer code

Data collection	Noldus Ethovison XT software, Noldus Observer XT
Data analysis	Noldus Ethovison XT software, Prism 8 GraphPad, BEDTools v. 2.17.0, RSEM v. 1.2.15, DAVID, QIAGEN Ingenuity Pathway Analysis, ImageJ, pClamp Software

For manuscripts utilizing custom algorithms or software that are central to the research but not yet described in published literature, software must be made available to editors/reviewers. We strongly encourage code deposition in a community repository (e.g. GitHub). See the Nature Research guidelines for submitting code & software for further information.

Data

Policy information about availability of data

All manuscripts must include a data availability statement. This statement should provide the following information, where applicable:

- Accession codes, unique identifiers, or web links for publicly available datasets
- A list of figures that have associated raw data
- A description of any restrictions on data availability

The data that support the findings of this study are available from the corresponding author upon reasonable request

Field-specific reporting

Please select the one below that is the best fit for your research. If you are not sure, read the appropriate sections before making your selection.

☒ Life sciences ☐ Behavioural & social sciences ☐ Ecological, evolutionary & environmental sciences

Life sciences study design

All studies must disclose on these points even when the disclosure is negative.

Sample size	No statistical methods were used to predetermine sample size. Sample size used is based on common and accepted size in the field.
Data exclusions	No animal or sample was excluded from the analysis
Replication	Results were replicated by using more than one batch of test animals or were validated by other technical means and methods. All replications were successful
Randomization	Experiments were randomized: mice order, items positions and samples loading were all randomized and counterbalanced
Blinding	All the investigators were blinded to genotype during experiments and outcome assessment

Reporting for specific materials, systems and methods

We require information from authors about some types of materials, experimental systems and methods used in many studies. Here, indicate whether each material, system or method listed is relevant to your study. If you are not sure if a list item applies to your research, read the appropriate section before selecting a response.

Materials & experimental systems

n/a	Involved in the study
☐	☒ Antibodies
☒	☐ Eukaryotic cell lines
☒	☐ Palaeontology
☐	☒ Animals and other organisms
☐	☒ Human research participants
☒	☐ Clinical data

Methods

n/a	Involved in the study
☒	☐ ChIP-seq
☒	☐ Flow cytometry
☒	☐ MRI-based neuroimaging

Antibodies

Antibodies used

Primary commercial antibodies used include TFII-I (Cell Signaling, 4562, 1:1,000) and Tubulin (Sigma, T5168, 1:10,000), CaMKIIa (1:400, Millipore, 05-532), GFP (1:3,000, Invitrogen, A11122), Sox10 (1:100, Santa-Cruz 365692), PDGFRa (1:1,000, Santa-Cruz 338), Olig2 (1:1,000, Millipore AB9610), CC1 (1:500, Calbiochem OP80), NeuN (1:1,000, Millipore MAB377), S100B (1:600, Sigma S2532) GAD67 (1:1,000, Millipore 5406), RFP (Abcam (Cat: ab34771), 1:200), OLIG2 (1:100, Millipore, AB9610) and APC (1:2, Calbiochem, OP80-100UG)
Secondary antibodies conjugated with Alexa488/555/647 (InvitrogenThermofisher, A-11094/A-21429/A-21245, 1:1,000), also secondary antibodies conjugated with Alexa488 and 568 (Invitrogen, A1101, A21245, 1:500).

Validation

These references used the primary antibodies used in the current study:
TFII-I (Cell Signaling, 4562, 1:1,000) - Guenat, D., Merla, G., et al. (2017)
Tubulin (Sigma, T5168, 1:10,000) - Pensato V, et.al. Journal of Neurology 262(5), 1376-1378, (2015)
CaMKIIa (1:400, Millipore, 05-532) - Yuan, Y; et al. Frontiers in cellular neuroscience 9 314 2015
GFP (1:3,000, Invitrogen, A11122) - Soyeon Park Et Al. PLoS ONE (2018)
Sox10 (1:100, Santa-Cruz 365692) - Zuo, H. et al. 2018. J. Neurosci. 38: 2359-2371
PDGFRa (1:1,000, Santa-Cruz 338) - Arellano, R.O. et al. 2016. Molecular pharmacology. 89: 63-74
Olig2 (1:1,000, Millipore AB9610) - Nishi, Y, et al. Development (Cambridge, England) 3286-93 2015
CC1 (1:500, Calbiochem OP80) - Bhat, R.V., et al. 1996. Glia 17, 169
NeuN (1:1,000, Millipore MAB377) - Bellesi, M et al. BMC biology 13 66 2015
S100B (1:600, Sigma S2532) - Bernardini N et al Journal of Cellular and Molecular Medicine (2012)
GAD67 (1:1,000, Millipore 5406) - Sharaf, A et al. Cell and tissue research 359 393-407 2015
RFP (Abcam, ab34771, 1:200) - Kothari P et al. J Cell Sci (2019)

Animals and other organisms

Policy information about studies involving animals; ARRIVE guidelines recommended for reporting animal research

Laboratory animals	All mice were on C57Bl/6 background, all males. Mice at ages E15.5, P1, P14, P30, P180 were used.

Wild animals	The study did not involve wild animals
Field-collected samples	The study did not involved field-collected samples
Ethics oversight	All animal-related work was performed under the guidelines of Division of Comparative Medicine (DCM), with protocol approved by the Committee for Animal Care (CAC) of Massachusetts Institute of Technology and was consistent with the Guide for Care and Use of Laboratory Animals, National Research Council 1996

Note that full information on the approval of the study protocol must also be provided in the manuscript.

Human research participants

Policy information about studies involving human research participants

Population characteristics	All information about the samples is in Supplementary Table 3
Recruitment	Human brain samples were obtained from the NIH Neurobiobank at the University of Maryland, Baltimore
Ethics oversight	MIT and the NIH Neurobiobank at the University of Maryland, Baltimore

Note that full information on the approval of the study protocol must also be provided in the manuscript.